Master's Thesis

Radboud University
Department of High Energy Physics

Detecting Dark Photons in Extensive Air Showers

Looking For New Physics with Radio Antennas

Author:
Bart Steeman

Supervisor:
Prof. dr. C.W.J.P. Timmermans

Second Reader:
Dr. H. Schoorlemmer

September 7, 2023

Contents

1. Introduction

In physics there are several phenomena that can not be explained by the standard model of particle physics. The most well known, and probably most glaring, mystery is the nature of dark matter, which comprises around 80 % of all matter in the universe [1]. It does not interact electromagnetically or through the strong force, and cannot be directly observed by us on Earth. Instead we rely on indirect methods that study the gravitational effects dark matter has on its cosmic surroundings. Many theories, like string theory and supersymmetry, predict new heavy particles that only interact weakly. These Weakly Interacting Massive Particles (WIMPs) are great dark matter candidates because if they exist they can naturally reproduce the right amount of dark matter currently present in the universe[1]. The search for these particles motivates much of the experimental efforts of the particle physics community, however to this day no evidence of them has been found at particle colliders like the Large Hadron Collider (LHC) which operates close to a center of mass energy of 14 TeV.

The future of WIMP dark matter is uncertain, and it invites physicist to explore some other interesting ideas. Our own particular exploration takes us to the hidden (or dark) sector, a name that would not be out of place as a location in a fantasy or adventure story. The hidden sector is comprised of a collection of hypothetical particles that are not charged under any of the standard model forces. They exist separately from our physical world, and can never directly interact with the particles we know. This sounds promising! It naturally delivers dark matter candidates. But this total separation between the hidden sector and standard model means we could never detect them, except through their gravitational interactions. However there is hope. There exist several mechanisms that can establish a connection between the physical and hidden sector, known as portals. One such portal is the Dark Photon, which arises as a gauge boson mediating an electromagnetic-like force between the hidden sector and visible particles. Because of their similar mathematical description it is possible for the dark photon and the photon to mix, meaning anytime a photon is produced in some interaction there is a chance that a dark photon is produced instead. Not only that, but a dark photon can also decay and produce standard model particles.

The dark photon was first described in 1985 in a paper by B. Holdom [2] [3]. The changes that need to be made to the mathematical description of the standard model are not difficult, and are described in the first chapter of this thesis. It has only two parameters: the mass of the dark photon and the strength of the mixing between the photon and the dark photon. The mixing strength is generally taken to be small. This means that the dark photon can be relatively stable, it only decays

after some macroscopic amount of time. Hypothetical particles with this behaviour are often grouped as Long Lived Particles (LLPs).

Many experiments, mainly particle colliders, have already placed limits on the dark photon parameters. Our exploration will take us outside of the lab. We will not look at accelerators as our source of high energy particles, or colliders for our interactions. We will exploit a natural source for these, cosmic rays.

Cosmic rays are high energy (reaching energies up to 10^{20} eV, much higher than is possible at the LHC) atomic nuclei that are produced and accelerated at explosive astrophysical events like supernovae[4]. They journey through the universe and after a long time some of them arrive at Earth. No longer safe in the relative vacuum of space they soon interact in the atmosphere, producing a massive cascade of particles known as an extensive air shower. The incredibly high cosmic ray energies lead to a large particle luminosity, and most of these particles are photons. This means the extensive air showers are potentially a great source of dark photons on Earth. Air showers can be detected in several different ways, but our focus will be on the radio signal that is produced by the charged particles in the shower. Dark photon production is rare, so we expect to need a detector with a large area to find a signal. Radio antennas are a relatively cheap way to cover this area, compared to particle detectors.

The goal of this thesis is to combine these two concepts and study the feasibility of the following dark photon detection method; A high energy cosmic ray arrives on Earth and produces an extensive air shower in the atmosphere. Somewhere within the body of the shower a dark photon is produced, that may carry a large fraction of the energy of the initial interaction of the cosmic ray in the atmosphere. The dark photon is long lived, and with a high Lorentz boost it can travel a significant distance through the atmosphere along the direction of the shower core. It does not interact with the atmosphere but will eventually decay into standard model particles. If the dark photon energy was sufficient (and the dark photon has enough atmosphere to travel through so it decays before hitting the ground) this will induce a secondary air shower. Both showers produce a radio signal, and because the second shower produced by the dark photon is closer to the ground (and the refractive index of the Earths atmosphere) the signal of the secondary shower arrives at the detector before that of the main shower. We should see two distinct peaks in the radio detectors with a time separation in the order of nanoseconds, depending on the production point of the dark photon and its decay length.

This is a completely novel method to detect dark photons. Working on something new is an exciting prospect, especially because of the way it combines theoretical particle physics and experimental astroparticle physics. But it also means that there are many questions to ask and answer, and a master internship has limited time to do so. Can we really see two distinct peaks in the radio signal? Are there background signals? Can we ever reach a statistically significant measurement? And are we sensitive in non-excluded areas of the parameter space? Using large amounts of Monte Carlo simulations as our weapon of choice we will answer the call to action and start on an adventure.

2. The Dark Photon

2.1 Quantum Field Theory

When we want to talk about exciting hypothetical particles like the dark photon it is important to understand some of the principles particle physics is based on. The zoo of particles that we know and understand (to a reasonable limit) are brought together into the **S**tandard **M**odel (SM)[5]. Here we group them based on their spin, charge, colour and mass into neatly defined groups. This is not purely based on empirical data, but on the underlying theory of the Standard Model: Quantum Field Theory (QFT). It generalizes quantum mechanics in so that it obeys the principles of special relativity. Particles are not described as classical objects with a fixed position in phase space, but as as excitations of fields following Lorentz-invariant equations of motion. A field essentially assigns a value to every point in a space. These fields can assign real or complex values, or even vector-like objects to every point in spacetime. Different types of fields will describe different types of particles: scalar bosons, vector bosons and fermions.

The name Quantum Field Theory implies that we somehow want to quantize the excited states of our underlying field to arrive at the description of particles. This is done in a similar way as with the simple quantum oscillator where we have ladder operators that increase and lower the energy eigenstate of the system. In QFT this behaviour ultimately follows from imposing certain (anti)commutation relations on the fields and their conjugate momenta. But since the concepts that are important for this thesis can be well explained using only classical field equations we will not be explaining canonical quantisation. Nor will we discuss perturbation theory, Feynman diagrams and related formulas will be used wildly without justification.

The dynamics and kinematics of particle fields are encoded in a Lagrangian equation. The Lagrangian allows you to find the equations of motion of the system by minimizing the action $S = \int \mathcal{L}(\phi, \partial_\mu \phi) d^4x$, where $\mathcal{L}$ is the Lagrangian density and ϕ is some field. Setting the variation of the action to zero leads to a set of field Euler-Lagrange equations that allow us to directly calculate the equations of motion from the Lagrangian density (defined in position space):

$$\partial_\mu \left(\frac{\partial \mathcal{L}}{\partial(\partial_\mu \phi)} \right) - \frac{\partial \mathcal{L}}{\partial \phi} = 0 \tag{2.1}$$

Inversely, if we know the equation of motion we can find a Lagrangian such that the e.o.m. are recovered by the Euler-Lagrange equations. As an example, we can consider free spin-$\frac{1}{2}$ fermions. We know that these obey the (Lorentz invariant) Dirac equation[6]:

$$(i\gamma^\mu \partial_\mu - m)\psi(x) = 0 \tag{2.2}$$

Where γ^μ are the gamma matrices and $\psi(x)$ is a Dirac field, a complex valued four dimensional vector in Dicarc space. With trial and error you can then find:

$$\mathcal{L}_{Dirac} = \bar{\psi}(i\gamma^\mu \partial_\mu - m)\psi, \ \bar{\psi} \equiv \psi^\dagger \gamma^0 \tag{2.3}$$

Where we need to define $\bar{\psi}$ in this way to ensure that the Lagrangian density is invariant under Lorentz transformations. The dynamic information is contained in the first term, and the second term is the mass term. The Dirac equation is easily recovered by applying the Euler-Lagrange equations with respect to the field $\bar{\psi}$.

2.1.1 Symmetry

A very important concept within particle physics is symmetry. This is a very broad statement, and applies broadly as well. There are the discrete **C**harge, **P**arity and **T**ime symmetries that are individually and pairwise broken in standard model interactions, but combine in the (for now still) obeyed CPT symmetry of particle interactions. Or you may know about continuous space-time translation symmetries that lead to the conservation of momentum and energy of a system.

How do we define a symmetry within QFT? It is a bit hard to conceptualize this, the classical idea of rotational or mirror symmetries of some object don't quite apply. We state that a symmetry is any (infinitesimal) transformation of the field that does not change the equations of motion. In terms of the Lagrangian this means that under the field transformations it may only acquire up to an additional four-divergence term, since those are automatically discarded by the Euler-Lagrange equations. A symmetry transformation on a field $\phi(x)$ with some infinitesimal parameter α should only lead an additional four divergence term:

$$\phi(x) \to \phi'(x) = \phi(x) + \alpha\Delta\phi(x) \tag{2.4}$$
$$\mathcal{L}(x) \to \mathcal{L}'(x) = \mathcal{L}(x) + \alpha\partial_\mu \mathcal{J}^\mu(x) \tag{2.5}$$

Noether's theorem states that such symmetries give rise to conserved currents. For example applying a space-time translation $\phi(x) \to \phi(x + \alpha)$ leads to conservation of the stress-energy tensor.

The standard model makes use of a special class of symmetries called gauge symmetries. These are local symmetries, meaning that the deformations to the field are dependent on the space-time coordinate. The infinitesimal transformations of equation 2.4 are applied globally to the entire field. But we can localize them by making the constant parameter α into a field $\alpha(x)$. These continuous local symmetry transformations are strongly linked to the concept of Lie groups. These categorize the local transformations as elements of a specific group, and describe the algebraic structure of the group elements.

The Standard Model is build on gauge symmetries. In terms of Lie groups particle interactions in the SM are invariant under the elements of the $SU(3) \times SU(2) \times U(1)$ group. Here $\times$ denotes the group product. $U(1)$ is the (unitary) commutative/abelian group of numbers on the complex unit circle. $SU(N)$ is the (special unitary) group of unitary matrices of dimension N, with a determinant of 1. The groups are linked to the fundamental forces: the strong and electroweak forces. In fact enforcing these symmetries on the matter fields of the standard model give rise to gauge fields, which are quantized to get the gauge bosons of the system. The amount of gauge fields is linked to the dimension of the respective group. We get $dim(U(1)) = 1$ hypercharge field B, and from $dim(SU(n)) = n^2 - 1$ eight gluons fields and three weak fields W^i. The weak fields and hypercharge field are subsequently combined through spontaneous symmetry breaking and electroweak mixing to get to the photon, Z and $W^{\pm}$ gauge bosons.

2.1.2 Quantum Electrodynamics

To illustrate the concepts explained in the last two sections we will take a closer look at the $U(1)_Y$ symmetry group. Here Y denotes the weak hypercharge, which is the conserved quantity related to this gauge symmetry. $U(1)$ does not only serve as an example, but it will help us understand the dark photon model. The name dark photon might already imply to the reader that it's origins might lie in similar symmetries as electrodynamics. We will start from the Dirac Lagrangian, equation 2.3. We want to transform our fields using elements of $U(1)$, that lie on the complex unit circle. We must also make sure to do this locally.

$$\psi(x) \to \psi'(x) = e^{i\alpha(x)}\psi(x) \tag{2.6}$$
$$\bar{\psi}(x) \to \bar{\psi}'(x) = \bar{\psi}(x)e^{-i\alpha(x)} \tag{2.7}$$

For the mass term $-m\psi\bar{\psi}$ it is easy to see that it is invariant under this transformation. But by demanding that the symmetry is local we have created a problem with the derivative in the first term of the Dirac Lagrangian. We can attempt to transform this term:

$$\begin{aligned}
&\bar{\psi}(x)\gamma^\mu\partial_\mu\psi(x) \rightarrow \bar{\psi}'(x)\gamma^\mu\partial_\mu\psi'(x) = \\
&\bar{\psi}(x)e^{-i\alpha(x)}\gamma^\mu\left(e^{i\alpha(x)}\partial_\mu\psi(x) + i\partial_\mu\alpha(x)e^{i\alpha(x)}\psi(x)\right) = \\
&\bar{\psi}(x)\gamma^\mu\partial_\mu\psi(x) + i\bar{\psi}(x)(\gamma^\mu\partial_\mu\alpha(x))\psi(x)
\end{aligned} \tag{2.8}$$

The Dirac Lagrangian is clearly not invariant, we get an extra term that depends on the derivative of $\alpha(x)$. To combat this problem we will replace the derivative with the gauge covariant derivative. This derivative contains a new gauge field A_μ that transforms under $U(1)$ in such a way that the extra term in equation 2.8 is counteracted and the Lagrangian becomes invariant.

$$D_\mu\psi(x) = (\partial_\mu + iqA_\mu(x))\psi(x) \tag{2.9}$$

$$A_\mu(x) \rightarrow A'_\mu(x) = A_\mu(x) - \frac{1}{q}\partial_\mu\alpha(x) \tag{2.10}$$

$$D_\mu\psi(x) \rightarrow e^{i\alpha(x)}D_\mu\psi(x) \tag{2.11}$$

So in the end, by demanding that we have a Lagrangian that is invariant under $U(1)$ transformations we end up introducing a new vector field $A_\mu(x)$ (the electromagnetic four-potential). It couples two fermion fields with a coupling strength of q, which corresponds to the (weak hyper-)charge of the fermions. As for any field in QFT we can quantize A_μ leading to it's corresponding gauge boson interpretation B. To complete the QED Lagrangian we unceremoniously add a kinetic term term for A_μ in a invariant manner, using the electromagnetic field tensor $F_{\mu\nu}$.

$$\mathcal{L}_{QED} = \bar{\psi}(x)\left(i\gamma^\mu D_\mu - m\right)\psi(x) - \frac{1}{4}F_{\mu\nu}F^{\mu\nu} \tag{2.12}$$

$$F_{\mu\nu} = \partial_\mu A_\nu - \partial_\nu A_\mu \tag{2.13}$$

So by starting from a interaction-less fermionic lagrangian and enforcing local $U(1)$ symmetry upon it we arrive at a new particle, a gauge boson related to the hypercharge. From equation 2.12 we can derive the well known Maxwell equations through the Euler Lagrange equations. The weak and strong forces can be introduced through the same process, but using the $SU(2)$ and $SU(3)$ Lie group symmetries.

2.2 The Hidden Sector

The dark photon is a part of beyond the standard model theories where there is a so called Hidden Sector. The Hidden Sector contains a group of new particles that

are not charged under any of the Standard Model forces. This means they do not directly interact with the known SM particles and are not directly detectable. The dark photon is one of the possible mediators that connects this hidden sector to the standard model. These are interesting theories because if these hidden particles are massive they are possible dark matter (DM) candidates, since of course they are dark (undetectable) and if they rarely decay into standard model particles they are stable enough to produce the correct relic density. Not only the particles in the Hidden Sector, but the dark photon itself has also been proposed as a DM candidate. They also provide new ways to search for new physics at collider experiments, which have yet to find the heavy dark matter candidates that are proposed by theories like supersymmetry. Dark photons with the specific masses and coupling strengths can also be used to explain several unsolved anomalies, like the 3.56 KeV galactic center spectral line, the positron excess in cosmic rays and the muon magnetic moment [3].

How can we hope to observe particles in a Hidden Sector if they are not charged under any of the SM gauge groups? This is possible through interactions of the Standard Model with so called portal particles. These are mediator particles of the hidden sector that all, through some mechanism, connect the hidden sector and the standard model. These interactions generally have small cross sections, but in theory allow us to observe a fingerprint of the hidden sector on our own physical world. We will never be able to detect these particles directly, we can only look through the portals to search for their existence. There are four well-studied portals, each differing in their spin and parity[7]:

- Neutrino portal (Dirac) [1].
- Higgs portal (scalar)
- Axion portal (pseudoscalar)
- Vector portal

The dark photon is such a portal, and unsurprisingly part of the vector portal family. And now it may also become clear why we focused on the $U(1)$ symmetry in the last section. When we add this vector portal to our theory we are essentially saying that the hidden sector are charged under some new $U(1)_X$ symmetry that behaves the same as the weak hypercharge in the standard model. We will take X to be some new universal charge number. [2] The new product group symmetry becomes $SU(3)_C \times SU(2)_L \times U(1)_Y \times U(1)_X$. Because we now have an additional $U(1)$ gauge boson we also need to extend the lagrangian. Similarly to the QED lagrangian we introduce a new gauge field A'_μ and a corresponding field strength tensor $F'_{\mu\nu}$. Now, when we write down the kinetic part of the lagrangian for the new

[1]The SM can be extended with right-handed heavy neutrinos. They mix with the left-handed neutrinos of the standard model, and provide a mechanism for the SM neutrinos to gain a mass term that's invariant under the SM symmetry. See also my bachelor's thesis: Sterile Neutrino Dark matter, Exploring the 3+3 Type I Seesaw Mechanism[8]

[2]This is not strictly necessary. For example there are theories where for X they take $B - L$, the baryon number minus lepton number, as the $U(1)$ global symmetry[9]. This can have an effect on the dark photon phenomenology.

gauge field, we can add a term that contains both the electromagnetic field strength tensor and that of the new field. This only possible because the $U(1)$ symmetries they stem from are abelian[10]. The additional terms in the lagrangian are:

$$\mathcal{L}_{dark} = -\frac{1}{4}F'_{\mu\nu}F'^{\mu\nu} - \frac{\epsilon}{2}F_{\mu\nu}F'^{\mu\nu} \tag{2.14}$$

The second term in equation 2.14 is known as the kinetic mixing term. Through this term the photon and dark photon are mixed [3] with a coupling strength ϵ. In practice this would mean that anytime a photon is created in some process there is a chance that instead a dark photon is produced. In general the ratio of the cross section (or decay width) of a process producing a photon to the same process producing a dark photon will scale with $\frac{\sigma_{dark\ photon}}{\sigma_{photon}} \sim \epsilon^2$[11].

ϵ is a free parameter, but should obviously not be too large. If so many dark photons would be created and we would have seen this in experiments. There is no fundamental reason for ϵ to be small. However, for example, we can choose to introduce terms in the UV renormalization of the theory to cancel out the kinetic mixing at tree level such that we only consider kinetic mixing that happens in loop corrections. In this case ϵ naturally takes on values in the order of $O(10^{-3})$. This can be further suppressed through several means, and in some string theories ϵ can naturally take on values in the order of $O(10^{-12})$[10]. So dark photon searches take place over a large range of possible mixing strengths.

In addition to the coupling parameter ϵ a second parameter is introduced, namely the dark photon mass $m_{A'}$. In principle the dark photon can be massless. However most experimental searches look for a massive dark photon, in part because it couples directly to the electromagnetic current J^μ. After diagonalizing the lagrangian we see:

$$\mathcal{L} \supset -e\epsilon J^\mu A'_\mu \tag{2.15}$$

The coupling of the massless dark photon to the electromagnetic current is less straightforward, and leads to a different phenomenology than for a massive dark photon. The massive case is also preferable our purposes, since we want the dark photon to be able to decay into a lepton-antilepton pair.

2.2.1 Production

Equation 2.15 tells us that the dark photon couples in exactly the same way to the standard model particles as the photon, albeit with a factor of ϵ suppressing the coupling strength. This means that the production channels are the same as for the regular photon. We only need to take into account that the processes are kinematically allowed for the chosen dark photon mass. Five important production

[3] The Z boson can also mix with the dark photon if we extend this to the full electroweak sector

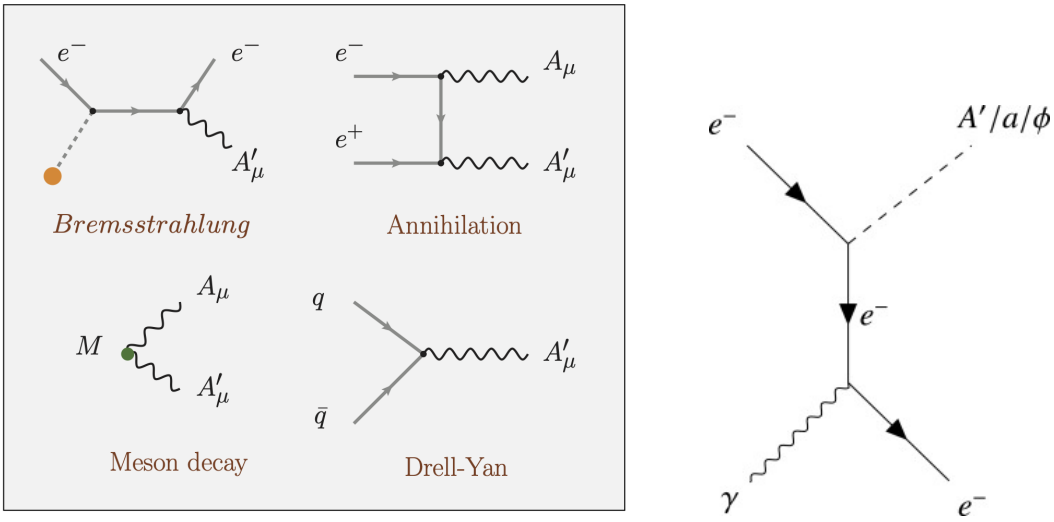

Figure 2.1: Left: The four dark photon production mechanisms from standard model particles. Right: Dark Compton scattering producing a dark photon, axion or scalar. Taken from [10] and [3].

mechanisms from standard model particles are shown in figure 2.1. We list some processes:

- **Bremsstrahlung** A charged particle (electron) radiates a dark photon while in the presence of an atomic nucleus Z: $e^- Z \to e^- Z A'$.
- **Annihilation** An electron-positron pair annihilates to a photon and dark photon: $e^- + e^+ \to \gamma A'$. If $m_{A'} \leq m_{e^-}$ two dark photons can be produced as well, but this carries an extra factor of ϵ and is therefore less favored. There is also the possibility of resonant production: $e^- + e^+ \to \gamma A'$.
- **Meson decay**. A neutral pion or heavier neutral meson decays to a photon and a dark photon: $m \to \gamma A'$. Similar to the annihilation case it is again possible to have two dark photons in the final products instead.
- **Drell-Yan** A quark-antiquark pair annihilate to produce a resonant dark photon: $q\bar{q} \to A'$.
- **Dark compton scattering** Similar to a normal compton scattering process, but with a dark photon in the final state: $e^- \gamma \to e^- A'$.
- **Dark matter annihiliation**. For a dark matter particle χ, which in our case would likely be a particle in the hidden sector, they can annihilate to a dark photon in the early universe if $m'_A \sim 2m_\chi$. If the dark photon is heavier it can still be produced off shell and decay into visible states.

2.2.2 Decays

When designing an experiment to search for dark photons an important choice has to be made; do you search for dark photons decaying to visible or invisible states. If the dark photon is heavier than twice the mass of the lightest particle in the

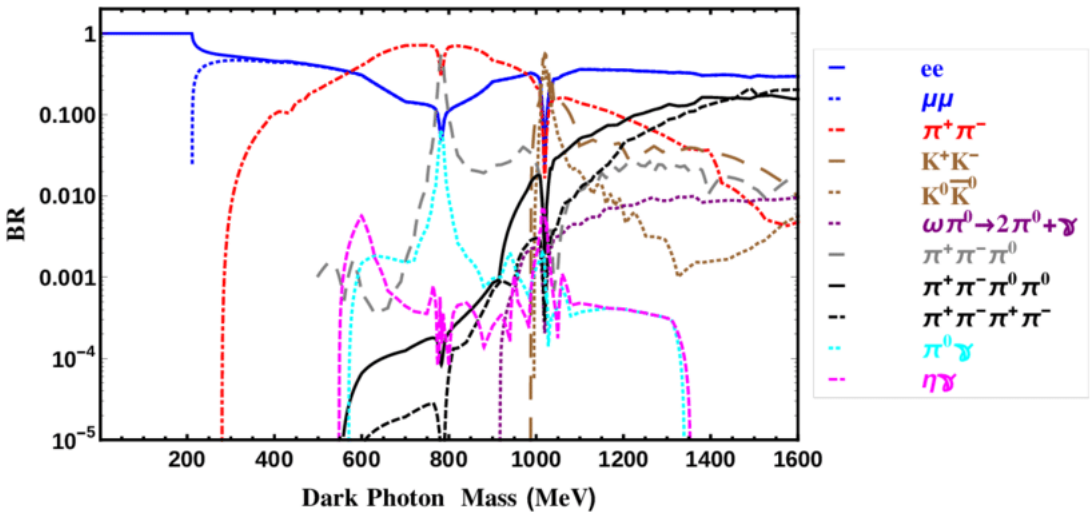

Figure 2.2: The branching ratios of dark photons decaying to visible states. Taken from [12].

hidden sector decays to the hidden sector are allowed. Depending on the coupling strength of the 'dark force' this channel can be dominant, especially since it is not suppressed by the mixing constant ϵ. In this scenario searches can be done by looking for missing mass, momentum and energy at fixed target and collider experiments.

In our research we make the choice to look at dark photons with only visible decay states. In this case the decay widths to lepton states are known analytically, and the decay to hadronic states is derived from the experimentally measured fraction $R_{\text{hadron}} \equiv \frac{\sigma_{e^+e^-\to\text{hadrons}}}{\sigma_{e^+e^-\to\mu^+\mu^-}}$. We have [10]:

$$\Gamma(A' \to l^+l^-) = \frac{1}{3}\alpha\epsilon^2 m_{A'}\sqrt{1-\frac{4m_l^2}{m_{A'}^2}}\left(1+\frac{2m_l^2}{m_{A'}^2}\right) \tag{2.16}$$

$$\Gamma(A' \to \text{hadrons}) = \frac{1}{3}\alpha\epsilon^2 m_{A'}\sqrt{1-\frac{4m_\mu^2}{m_{A'}^2}}\left(1+\frac{2m_\mu^2}{m_{A'}^2}\right) R_{\text{hadron}} \tag{2.17}$$

Figure 2.2 shows the branching ratios of dark photons decaying to visible states over a large range of dark photon masses. Decay to an electron-positron pair is only possible when $m'_A \geq 2m_e \approx 1\ MeV$. As we can see the decay widths are suppressed by a factor ϵ^2. This means that for small values of ϵ the dark photon acquires a significant proper lifetime, which can be scaled to some common values for ϵ and $m_{A'}$[3]:

$$c\tau = \frac{1}{\Gamma} = \frac{3}{N_{\text{eff}} m_{A'}\alpha\epsilon^2} \sim \frac{80\ \mu\text{m}}{N_{\text{eff}}}\left(\frac{10^{-4}}{\epsilon}\right)^2\left(\frac{100\ \text{MeV}}{m_{A'}}\right) \tag{2.18}$$

Where N_{eff} is the effective number of decay channels (which will be one in our simulations). This puts the dark photon in the category of Long Lived Particles (LLP's), which are hypothetical particles with macroscopic decay lengths (when

boosted). This opens up some additional detection methods, in addition to the more traditional resonance searches in collider experiments.

2.2.3 Detection and Limits

A lot of work has already been done on limiting the (theoretically not very limited) $\epsilon - m_{A'}$ parameter space. Often this is done by reanalyzing existing experimental data. Over the entire parameter space limits can be derived from a long list of physical phenomena. Especially in the low dark photon mass region (with decays to only invisible states) the list of existing limits is exhaustive. They can be derived from an incredibly wide range of physics, like: energy transport effects in stars, direct dark matter searches (like XENON), the hyperfine splitting in hydrogen atoms, the cosmic microwave background and light-shining-through-wall experiments searching for axions. However in the case of dark photons that decay to visible states the strongest limits are derived from looking for dilepton tracks from decaying dark photons in collision and beam dump experiments [13]:

- **Colliders** Collider experiments look for dark photons in resonances of electron and muon pairs. They are generally sensitive for high values of ϵ, since the dark photon has to decay relatively close to the primary interaction. If the proper lifetime is too large the decay would take place outside the detector volume. Different production mechanisms are used depending on the particle content of the collision beam. Figure 2.3 shows the limits derived from the NA48/2, A1, BaBar, KLOE and LHCb experiments.

- **Beam Dumps** In beam dump experiments dark photons are produced by colliding a beam (electron, proton) on a fixed target material. Behind the target a dump is placed, which is some amount of material that can absorb the particles produced in the fixed target collision. A dark photon with a sufficient lifetime will move through the dump volume unattenuated. A detector is placed behind the dump to look for the decay products of the dark photon. These experiments are sensitive to lower values of the mixing parameter because of their high particle luminosity. Figure 2.3 shows results from beam dump experiments at SLAC, Fermilab and CHARM.

- We also have additional limits from the experimental measurements of the electron magnetic moment and from energy losses measured in supernova SN1987A.

The research in this field is very active, and there are many proposed upgrades to existing experiments, like at LHCb, or future experiments like FASER (ForwArd Search ExpeRiment) that will continue the search for the dark photon and similar hypothetical particles. Figure 2.4 shows the projected sensitivities of these future measurements.

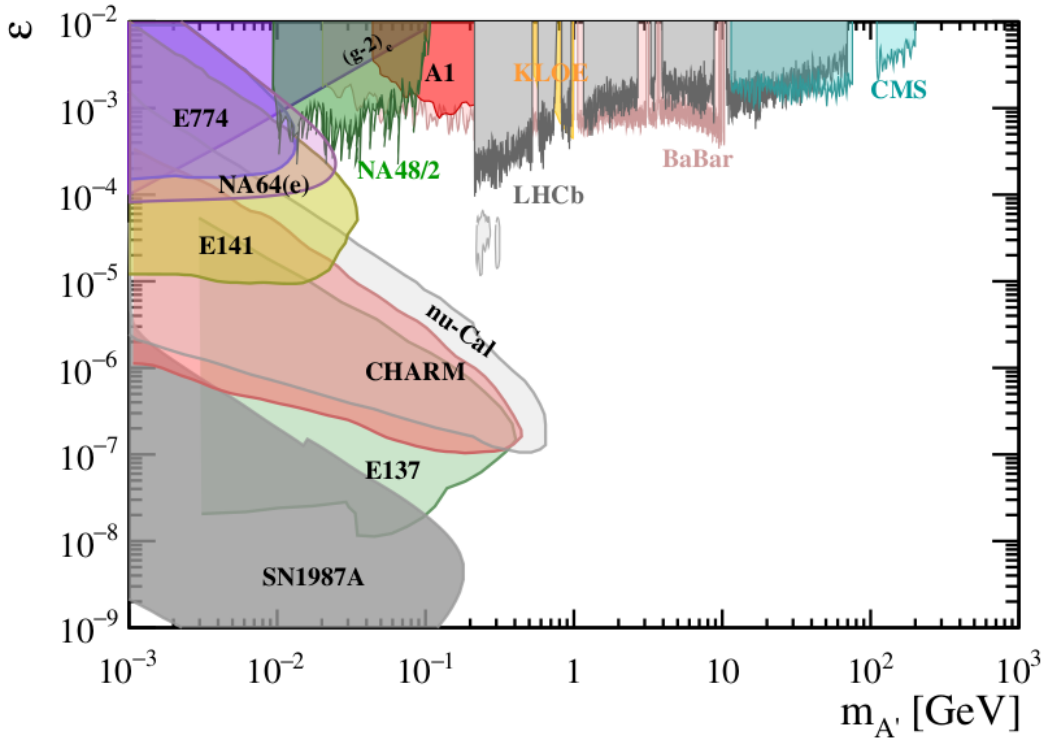

Figure 2.3: Existing limits on the dark photon mass and mixing parameter for massive dark photons decaying to visible states. Taken from [10].

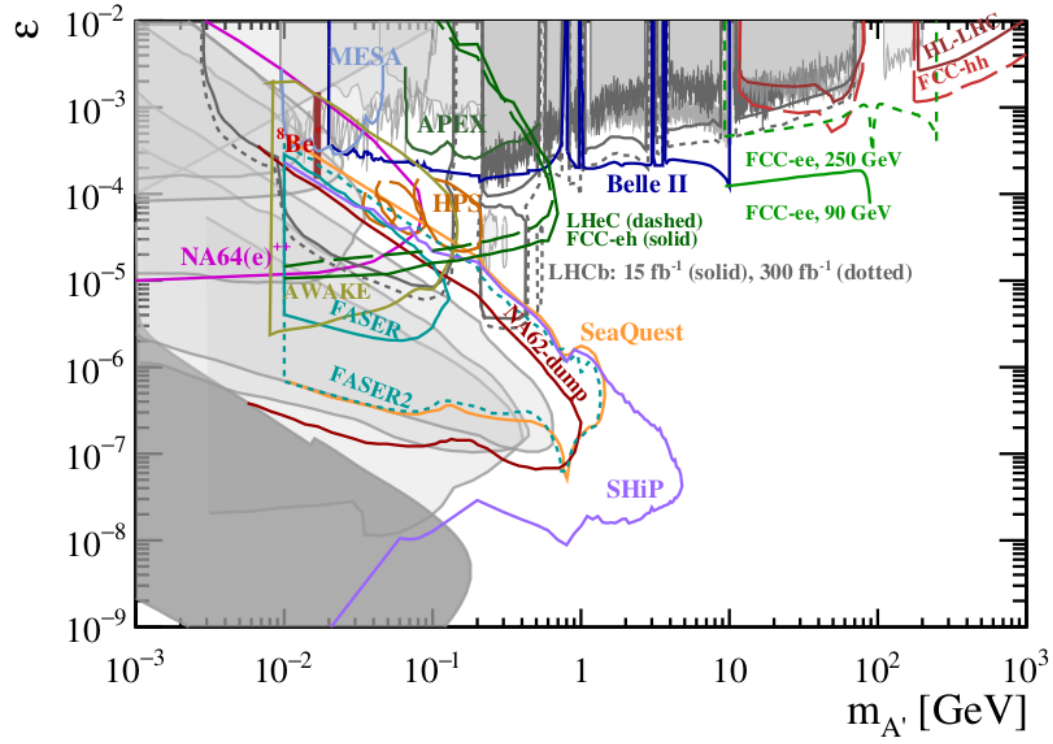

Figure 2.4: Projected limits on the dark photon parameter space from future measurements. Existing limits are shown in grey.

3. Extensive Air Showers

Existing limits [1] on the dark photon parameters have largely been derived with particle accelerator experiments. The low cross sections involved with dark photon production make it necessary to produce and analyze many femtobarn^{-1} of data, and the experiments at the LHC, Fermilab and SLAC provide high intensity beams in a controlled and clean setting. There exists another 'reliable' source of high energy particles that we might be able to use: cosmic rays.

3.1 Cosmic Rays

Cosmic rays are ionized nuclei moving through space at relativistic velocities [4]. They exist over a broad spectrum of energies, up to $\mathcal{O}(10^{20})$ eV and have several possible sources. They have been linked to solar activity, supernova remnants, gamma ray bursts and more, but certainly for the highest energy cosmic rays their origin and method of acceleration are not yet fully understood. Most cosmic rays will stay inside the galaxies in which they are created, where their paths are bent by the galactic magnetic fields. In this time they may interact with the interstellar medium and occasionally produce secondary cosmic ray particles, often in the form of (anti)protons. In the milky way cosmic rays may travel up to thousands of times the thickness of the galactic disk before they undergo some process. Because of this cosmic rays do not point back to their sources. Sources can perhaps be identified by studying high energy photons and neutrinos, since they are not deflected by the magnetic fields. However the arrival time of a sources neutral particles and cosmic rays on Earth will differ by thousands of years, and can not be correlated with any neutral particles from transient events.

Some cosmic rays will in fact find their end in or above the Earths atmosphere, where we can detect them. Figure 3.1 shows the differential cosmic ray flux. It falls roughly exponentially with a factor of -2.7. There are several features where the factor changes slightly, like around the knee and ankle shown in the figure. Cosmic rays at energies around 10^{11} eV arrive at Earth with a rate of one particle per square meter per second. These can be measured with satellite or balloon based experiments (like PAMELA), containing calorimeters and spectrometers that allow us to accurately determine their mass and charge. At these energies we know the relative abundance of cosmic ray nuclei, ranging from single protons to iron nuclei. For higher energy cosmic rays however we are at the mercy of indirect detection methods. The flux becomes too low to get significant measurements from satellites,

[1] At least the ones relevant to a dark photon with $m'_A \geq 1$ MeV, decaying to visible states.

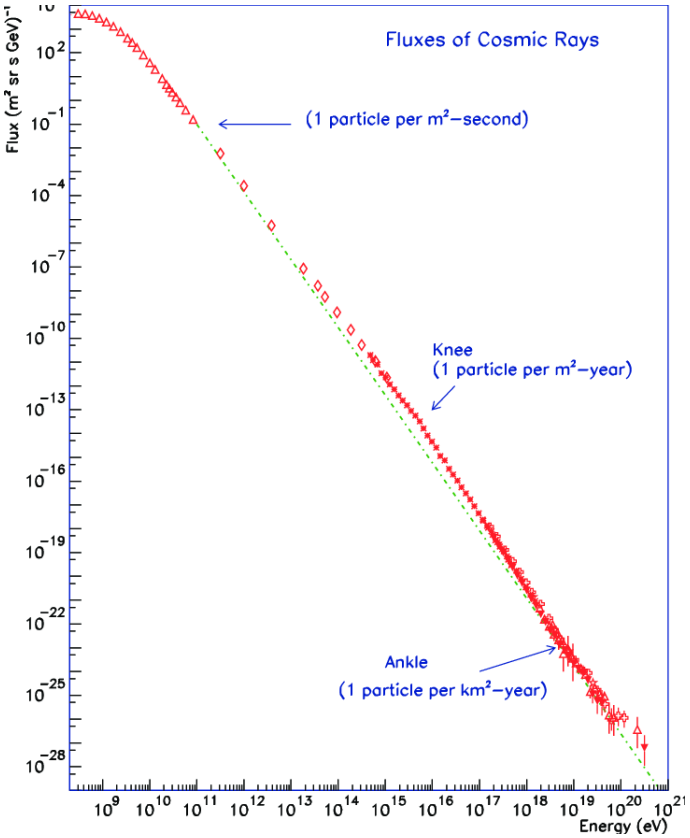

Figure 3.1: The differential cosmic ray spectrum. It shows the particle flux at Earth for several cosmic ray energies. Taken from [14]

that suffer from limited available detector volume.

The origin, particle composition and propagation of (ultra-high-energy) cosmic rays are the open questions that drive much of the current research in the field of astroparticle physics. We will leave it at this short introduction however. In this thesis we can not and do not contribute towards answers to these mysteries, we merely make use of the existence of cosmic rays for our own benefit.

3.2 Air Showers

High energy cosmic rays (roughly upwards of $E_{\text{primary}} = 10^{15}$ GeV[15]) can not be directly detected due to their low flux. However we can use the Earths atmosphere to our advantage. When a high-energy cosmic ray enters the Earths atmosphere it will interact with an air molecule. The products of this interaction will travel further through the atmosphere and interact again after some distance, determined by some characteristic interaction length. This process repeats itself, producing a cascade that stretches through the atmosphere. This is what we call an extensive air shower. The point of first interaction is indicated with X_0 (more information about the units used is found in section 3.2.1). This interaction point fluctuates between showers with identical parameters because of the inherent stochastical nature of particle interactions. The average of X_0 is influenced by the primary energy and cosmic ray mass. A high energy shower or a more massive nucleus will have a larger

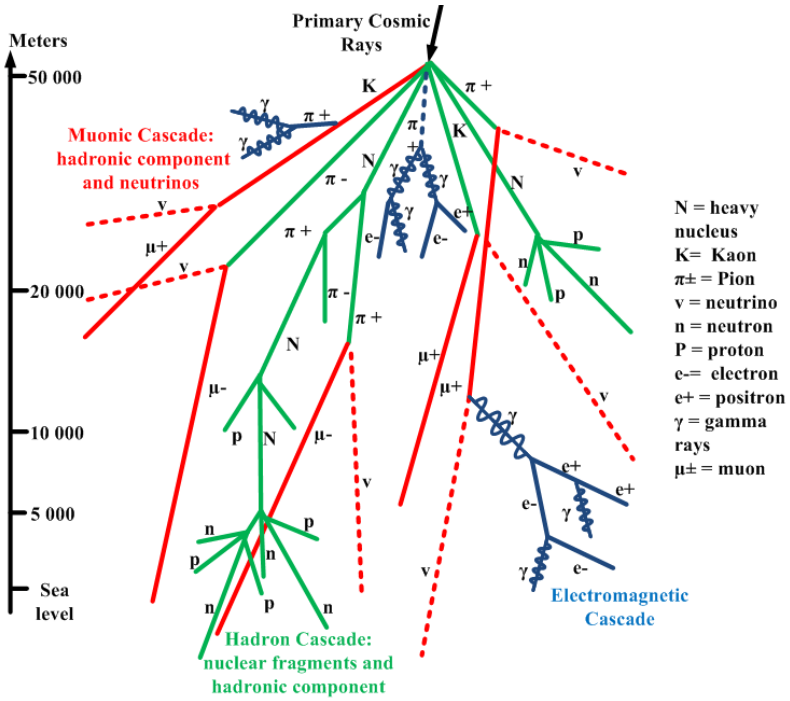

Figure 3.2: A schematic representation of the interactions taking place inside an extensive air shower. The electromagnetic part is represented in blue, the hadronic part in green and the muonic part in red. Note that the number of particles in each section does not relate to the general ratio between the three parts of an air shower. Taken from [16].

cross section with molecular nitrogen, and thus have a lower penetration depth into the atmosphere.

Within the shower we define three parts. A hadronic core, an electromagnetic part largely induced by photons produced in neutral pion decays, and the more stable muonic part that come from low energy charged pions and kaons decaying. Most of the energy of the initial cosmic ray ends up within the electromagnetic part of the shower. Here photons, electrons and positrons are mainly produced through bremsstrahlung and pair production. Figure 3.2 gives an overview of the most common processes in an extensive air shower. After enough interactions the energy divided among the electrons and positrons falls below the critical energy, where energy losses by ionization dominate energy losses through radiative processes. At this point only few new particles are created and the shower energy dissipates into the atmosphere through ionization. At this point the shower will have reached a peak in the total number of particles, denoted by its slant depth in the atmosphere $X_{\max}$ (see section 3.2.1). The total number of particles at $X_{\max}$ scales linearly with the primary cosmic ray energy. The average $X_{\max}$ for a shower with at a certain primary energy depends on the mass of the cosmic ray. Heavier nuclei will reach their maximum earlier in the atmosphere [17]. They interact earlier in the atmosphere (because of a higher interaction cross-section) and the nucleus breaks up to form essentially several lower energy sub-showers. Depending on the cosmic ray energy, the primary interaction depth and the angle of the shower (denoted by the zenith angle θ_z relative to the normal of the Earths surface) shower particles may reach the Earth. In figure 3.4 we can clearly see that the electromagnetic

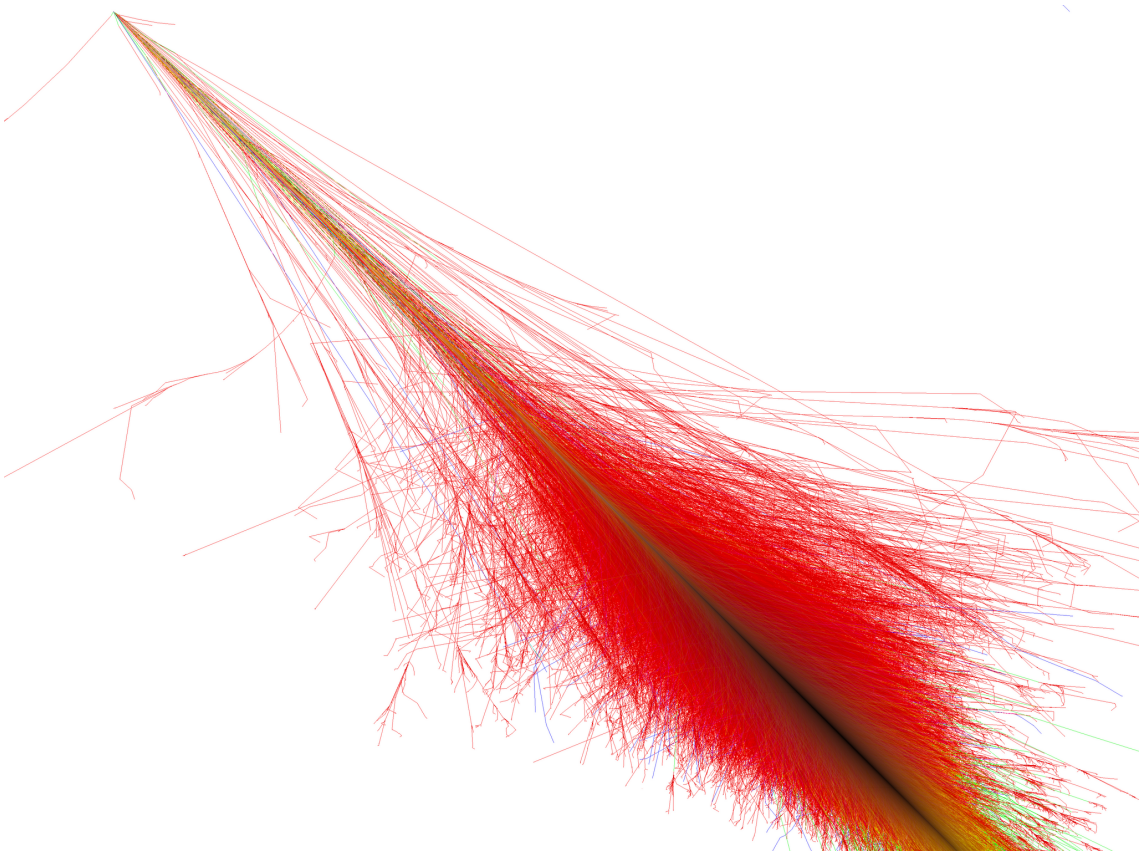

Figure 3.3: A CORSIKA simulation of an air shower induced by an 10^15 *eV proton. The proton entered the atmosphere under a zenith angle of* $\theta_z = 45°$*. Taken from* `https://www.iap.kit.edu/corsika/`

part dominates the particle content of the shower, and that for a ultra-high-energy shower ($E_{\text{primary}} \leq 10^{18}$ eV) a significant amount of particles reaches the Earth (at the atmospheric depth of the Pierre Auger Observatory). Figure 3.3 shows a simulated proton induced shower. From this figure we can gain some intuition on the general shape of an extensive air shower. Note the high number of products from the first (hadronic) interaction. The longitudinal shape of air showers show similar behaviour among all showers, and can be parameterized by the so called Gaisser-Hillas function [4].

3.2.1 Atmospheric and Slant depth

In figure 3.4 the vertical axis of the longitudinal distribution plot is the atmospheric depth, given in g/cm^2. This unit is derived by taking a path integral over the atmospheric density profile radially away from Earth (vertical showers). This is a useful unit because we are interested in particles interacting with the molecules in air. The atmospheric density profile is generally modelled with an exponential distribution, decreasing radially away from the Earth surface. The zero point for the atmospheric depth is set at an infinite radial distance from the earth. The atmospheric depth at the ground is dependent on the height above sea level. At sea level the atmospheric depth is 1080 g/cm^2. While for example the atmospheric depth at the Pierre Auger Observatory is around 820 g/cm^2.

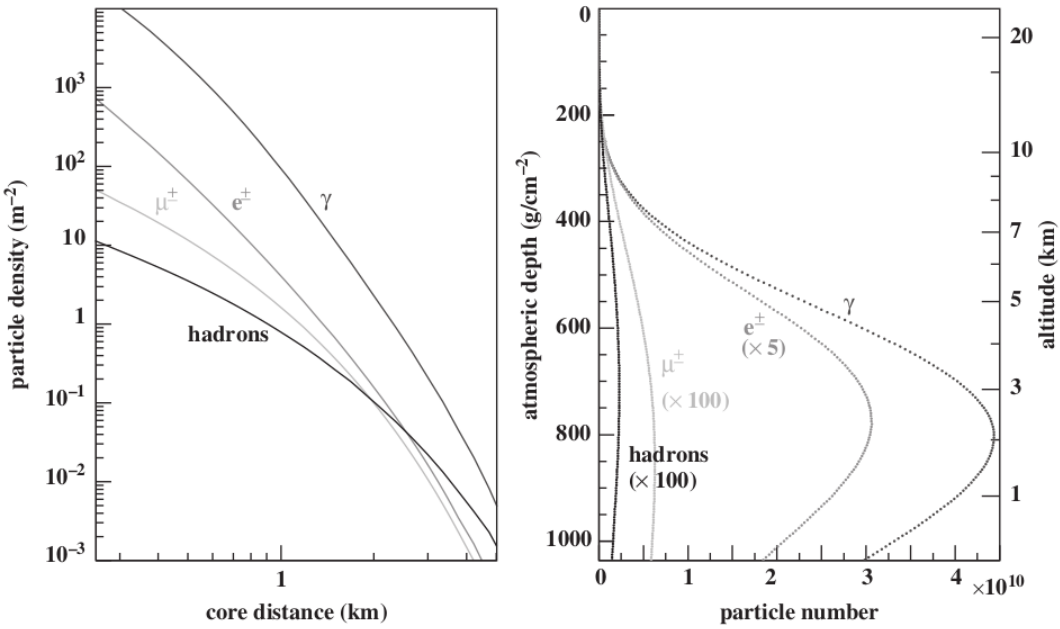

Figure 3.4: Averaged shower distributions of vertical air showers with a primary cosmic ray energy $E_{primary} = 10^{19}$ eV. Left: The lateral distribution on the ground at 820 g/cm^2. Right: The longitudinal shower distribution. Taken from [4].

Slant depth is a related unit, where the integral is not performed radially away but along the direction of the air shower development (for a vertical shower the slant depth and atmospheric depth are the same). The direction of a shower is parameterized with an azimuthal angle and the zenith angle θ_z. For a vertical shower the zenith angle is zero. When a shower enters the atmosphere under a higher zenith angle it has to travel through the atmosphere longer to reach Earth, and the integral over the exponential density becomes less straightforward. Integrating along the shower axis gives the slant depth. Every point along a shower has both a slant depth and vertical/atmospheric depth, the slant depth being calculated along the shower axis and the vertical depth radially from the Earths surface, through the point on the shower axis, and to the top of the atmosphere.

3.2.2 Detection methods

There exist several methods to detect the cosmic ray induced air showers. They have the goal to determine the arrival direction of the cosmic ray, its primary energy and mass. This has to be done indirectly by studying the air shower. We describe a few methods here [15], but leave the radio detection of air showers to its own section. We use the Pierre Auger Observatory as the example of how these methods are employed in practice.

- **Fluorescence Detectors** When the air showers pass through the air they excites nitrogen molecules, who then radiate away photons close to the visible spectrum when they fall back to their ground states. On a clear night these can be detected using telescopes. By measuring the amount of fluorescence

light emitted along the shower track the longitudinal shower development can be determined. By integrating the total emitted fluorescence we can find the total shower energy. Auger employs six telescopes at four different sites each. Because of the clear night condition they have an uptime of around 10%.

- **Particle Detectors** Particle detectors can look for shower particles arriving on the ground. The main types of detectors used are Water Cherenkov detector tanks and scintillators. They are placed on the surface in a regularly spaced grid. Depending on the desired energy range the detectors are placed close to each other for low energy air showers (which have a small footprint on the Earth) and further apart over large areas for the detection of high-energy air showers. The Pierre Auger detector has 1660 Cherenkov tanks placed in a triangular grid with 1.5 km spacing over an area of 3000 km^2. Auger is sensitive to air showers above 10^{17}GeV [17]. The shower footprint on the detector area and the relative arival time of particles in the individual detectors can be used to determine the arrival direction of the cosmic ray. Combining information about $X_{\max}$ from fluorescence detectors and the relative fraction of muons in the detectors is an indicator for the cosmic ray mass. However to infer the mass from these parameters we rely on data from Monte Carlo simulations of air showers. These rely on hadronic models that extrapolate from experimentally determined hadronic cross sections in accelerator experiments. This makes calculating the mass from shower observations model dependent and prone to large uncertainties. With the Auger Prime upgrade [18] organic scintillators are placed on top of the existing water tanks. These have very different responses to specific particles compared to water Cherenkov detectors. Combining the measurements from the scintillator and water Cherenkov tanks allows for a more precise measurement of the ratio between the muonic and electromagnetic content of the shower. This leads to a better determination of the composition of the cosmic ray beam.

- **Atmospheric Cherenkov Telescopes** The highly relativistic charged particles that are created at the start of an air shower can produce Cherenkov radiation in the atmosphere. The cherenkov radiation is emitted within a forward beaming cone. Optical telescopes capture this light, and can reconstruct the shower from the shape and intensity of the cherenkov ring. This technique is now more often used for extensive air showers induced by high energy photons. An example is the H.E.S.S. telescope in Namibia, which employs an array of five optical telescopes.

3.2.3 Radio Detection

Because of the incredibly low flux of ultra-high-energy cosmic rays it is necessary to build detectors with incredibly large surface areas to measure them. Practical and budgetary considerations make it a difficult prospect to build surface detector type experiments with significantly larger areas than the Pierre Auger Observatory or Telescope Array [19] (currently consisting of 500 scintillators on an area of 762 km^2, but they are expanding the area by a factor of 4). A possible solution to this problem is to be found in the radio emission of air showers.

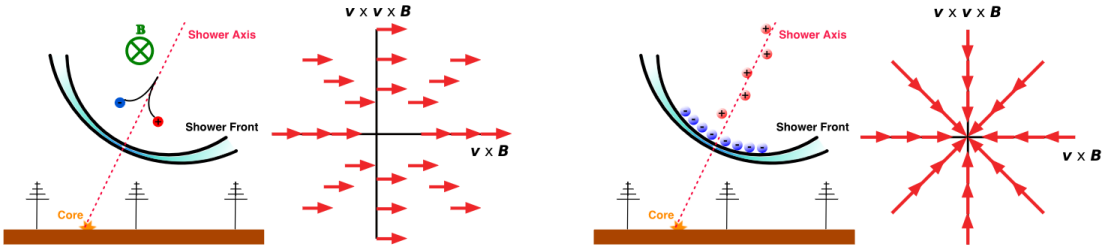

Figure 3.5: A visual representation of the two main radio emission mechanisms of air showers and the resulting polarisation. Left: the geomagnetic emission. Right: the charge excess mechanism. Taken from [20].

There are two main mechanisms that contribute to the radio emission of air showers[20]:

- **Geomagnetic** The dominant contribution is produced by the interaction of the charged particles in the shower with the Earth's magnetic field. Through the Lorentz force a net drift of charged particles (with a component) perpendicular to the shower axis is induced. The strength of the current changes over time due to the increase and subsequent decrease of the number of charged particles in the longitudinal development of the shower. This varying current induces emissions in the radio frequency range. It contributes around 90% of the total radio emission.
- **Askaryan/charge excess** A second contribution comes from an excess of electrons in the shower front compared to the 'tail' of the shower. When the shower front passes through the atmosphere molecules are ionized, and the freed electrons are carried forward with the front. The ionized molecules stay behind, setting up a net charge difference. This difference again changes over the lifetime of the shower, resulting in radio emission. This explains most of the remaining 10% of emissions.

An important detail is that individual charged particles all add to the radio emission. If they interfere destructively we will see no signal. It turns out that the individual signals add coherently in the $30 - 80$ MHz range. The total radiated power of the radio signal in this range thus scales linearly with the number of charged particles, and quadratically with the primary cosmic ray energy. The geomagnetic and charge excess emissions do have different polarisations, as shown in figure 3.5. This can lead to destructive or constructive interference depending on the location of the detector relative to the shower axis.

It has been shown that a detector consisting of a surface array of radio antennas (sensitive in the $30 - 80$ MHz range) can reconstruct important shower parameters [20]. As already stated the radiated power scales quadratically with the primary shower energy. The depth of the air shower influences the lateral distribution of the radio footprint. The arrival direction of the shower can be constructed from the relative arrival time of the radio signal in individual antennas. $X_{\max}$ can also be determined by looking at the lateral distribution of the radio signal on the ground. An analysis by the Tunka-Rex achieved a $X_{\max}$ resolution of 40 g/cm^2, which is

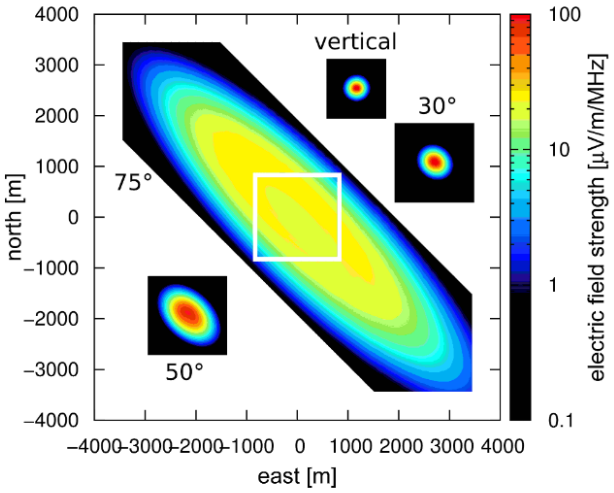

Figure 3.6: The radio footprint of extensive air showers for various shower inclinations (zenith angles), from CoREAS simulations. Taken from [21]

not yet competitive with the resolution of fluorescence detectors, which is around $20 - 25$ g/cm^2 [20].

Being able to use only radio antennas to measure air showers is an important step for future detection of ultra-high-energy air showers. The relatively cheap cost and easy upkeep of the radio antennas makes it possible to design detector arrays with much larger surfaces. GRAND (Giant Radio Array for Neutrino Detection) is a proposed radio detector that aims to cover a total area of 200.000 km^2 with 200.000 antennas [21][22]. This is a factor 66.67 larger than the Pierre Auger Observatory. It aims to be sensitive to showers with energies upwards of $10^{17}eV$. This can be done with a relatively sparse grid of antennas by only looking at highly inclined (high zenith angle) showers, which leave a much larger radio footprint on the Earth's surface compared to vertical showers. Figure 3.6 shows the radio footprint of high-energy air showers for several different inclinations. Radio emissions from highly inclined air showers cover a much larger area on earth, and can thus be effectively sampled with a much sparser antenna grid.

3.2.4 Air Shower Simulations

In this work we will need to simulate many extensive air showers and the radio emission produced by these showers. There are several software packages available that employ Monte Carlo methods to simulate the the individual particle tracks and interactions, like CORSIKA and AIRES. We will be using a modified implementation of AIRES version 19.04.08 [2][23]. AIRES was first released in 1997 and is written in FORTRAN77. It has been continually maintained and updated to this day.

[2] A new version of AIRES, 19.04.10 was published during my internship. This version added a python interface to cal the AIRES object library written in FORTRAN. This might be a helpful feature for future students working with AIRES, since they generally have more experience with python.

AIRES simulates air showers based on several input parameters given by the user. These can be set dynamically in the command prompt, or collected in a input file. These include:

- The number of simulated showers. If you set this larger than one you can choose to only see averaged observables over all showers or the individual simulation results.
- The primary shower energy (either a set value or randomly sampled from an exponential distribution with some slope)
- The primary particle inducing the air shower (photon, neutrino, proton...iron)
- The zenith angle of the incoming primary particle (or a range of angles between $0°$ and $89.99°$, which is then sampled with a sine distribution).
- Using the 'special primary' routine it is possible to simulate more complex initial configurations of particles. For example a 'regular' proton can be placed at some initial interaction point and a high energy photon can be placed manually some distance along (or off) the shower axis.

AIRES uses random sampling methods to determine the track and eventual fate of the shower particles. It determines the outcome of electromagnetic processes like pair production, bremsstrahlung and compton scattering. It determines when unstable particles like pions and muons decay. Finally it takes into account the propagation of charged particles through the atmosphere, taking into account radiative and ionizing processes. Some hadronic processes, like elastic scattering and fragmentation, are done by AIRES. But for inelastic processes the program contains several hadronic collision packages like EPOS, QGSJET and SIBYLL. These apply different models to extrapolate collider data of hadronic cross sections to the much higher energies that occur in ultra high energy cosmic rays, introducing model dependence to the air shower simulations. The standard AIRES installation uses SIBYLL 2.3, as do we in this work. AIRES uses the US standard atmorsphere model to determine the atmospheric density. Other atmospheric models can be integrated if needed.

To fully track all particles in a high energy air shower would take an immense amount of calculations (A 10^{20} eV shower contains in the order of 10^{11} particles, all requiring multiple Monte Carlo calculations). To reduce the computation time a thinning procedure is applied. A cut off energy E_{th} is given as an input parameter of the simulation. When a shower particle above E_{th} undergoes some process and the products fall below the thinning energy, they are kept with a chance of $\frac{E_{\text{product}}}{E_{th}}$, and otherwise discarded from the simulation. The particles that are kept in the simulation gain an increased weight factor inverse to the acceptance probability. For every particle below the thinning energy that interacts only one interaction product will be kept in the simulations, with the acceptance probability determined by its relative energy fraction, ensuring that the number of particles below the thinning energy cannot increase. The simulation becomes less intensive the higher the thinning energy is set (relative to the primary energy). This thinning algorithm ensures that any averaged shower observables will be the same regardless of the chosen thinning

energy. It does strongly influence the amount of fluctuations in some outputs, like the number of (charged) shower particles along the longitudinal shower development.

AIRES has three levels of outputs. The first level is the summary report generated after every simulation. This gives some technical information about the simulation, shows the input parameters and shows some observables like the vertical and slant depth of the first interaction point and $X_{\max}$, and the number and energies of particles that reach the ground. The second layer consists of a list of output tables that can be generated by the program when requested in the input file. This includes the lateral, longitudinal and energy distributions of many individual particles. This includes particles like electrons/positrons and Kaons. Less stable particles like the neutral pion and the tau are however not included. There are also tables available for all shower particles, or only the charged particles.

The third layer consists of compressed data files that store information on the level of individual particles. One file stores all information of particles that have reached the ground (.grdpcles), and the other stores information on particles during the shower development (.lgtpcles). These files can be read out with custom FORTRAN or C scripts using the AIRES object library. An important note is that particles are only saved in the .lgtpcles file if they cross an observation level. AIRES draws up to 510 planes in the atmosphere (at regular distances apart with standard settings). A particle is recorded the moment it crosses an observation level. The number of observing levels influences the final size of the longitudinal tracking file. Another space saving measure in the longitudinal tracking file is that after the first 20% of the shower development particles close to the shower core are not stored in the compressed file. This makes sense if you are only interested in the lateral spread of the shower at any point in its development. If you need to study the longitudinal development of the highest energy particles in the shower (which are generally close to the shower core due to the high lorentz boost factor) you can change this setting by including the RLimsFile directive in the input file (see the AIRES manual [23]).

Decays of unstable particles like the neutral pion are taken into account in the shower simulation, but since they almost immediately decay to photons they will not cross any observation levels and will not be saved in the longitudinal tracking file.

ZHAireS

The calculation of the electromagnetic radiation of the air shower is done by ZHAireS (A combination of Aires and ZHS). ZHS is a code by Zas-Halzen-Stanev to calculate the emissions from the individual charged particle tracks in the air showers. It calculates this parallel to the shower calculations done by AIRES. It outputs the electric field and potential components at some location on the ground where an antenna would stand. This location can be given in real Earth coordinates, and it will use the local geomagnetic field to calculate the radio emission. One can place a single antenna or an entire grid, producing output files for every individual antenna in the grid. The output of the simulation can be recorded in the time and frequency domains. There are some restrictions one needs to take into account when running ZHAireS. Only one shower can be simulated at the time (i.e. the num-

ber of showers input directive must be set to one). It is not supported to provide a range of primary energies or azimuth and zenith angles, they must be set explicitly.

One must also take into account that the thinning energy used for the shower simulation will influence the ZHAireS output. A high thinning energy results in stronger fluctuations in the number of charged particles in the longitudinal development of the shower. These fluctuations also cause increased noise in the radio signal since that depends on the time derivative of the number of charged particles in the shower. This is especially problematic when looking for low intensity radio signals in time domain outputs, since they may be buried in the simulation noise.

4. The Experiment

Now that we described dark photons and air showers in some detail we have all the ingredients to discuss the proposed experiment. As stated in the introduction the physical signal begins with a extensive air shower induced by a high energy cosmic ray, say $E_{\text{primary}} \gtrsim 10^{16}$ eV. Many photons are created in the air shower, in figure 3.4 we see that photons easily outnumber all other particles. Almost all of them are produced in neutral pion decays: $\pi^0 \to \gamma\gamma$ and through Bremsstrahlung. A small amount of photons is created in η meson decay.[4]. In the dark photon model anytime a photon would be produced in a standard model interaction there is a chance of a dark photon being produced instead. The branching ratio of a neutral pion decaying to a photon and a dark photon depends on the mixing parameter ϵ and the dark photon mass and is given by [24]:

$$B\left(\pi^0 \to A'\gamma\right) = 2\epsilon^2 \left(1 - \frac{m_{A'}^2}{m_{\pi^0}^2}\right)^3 B\left(\pi^0 \to \gamma\gamma\right) \tag{4.1}$$

Where $B\left(\pi^0 \to \gamma\gamma\right)$ is 98.8%[25]. The same formula holds for η decay, but the branching ratio of $\eta \to \gamma\gamma$ is around 39%. If the mixing parameter is taken ro be small the factor ϵ^2 ensures the branching ratio is also small, and only few dark photons are produced.

A highly boosted dark photon can travel a significant distance through the atmosphere before decaying. The mean decay length of the dark photon in the atmosphere is given by:

$$d_{A'} = \gamma\beta c\tau = \frac{p_{A'}}{m_{A'}} c\tau \tag{4.2}$$

Where the proper decay length $c\tau$ is given by equation 2.18. For example, a dark photon with a mixing parameter of 10^{-4}, mass of 100 MeV and an energy of 10^{16} eV has a mean decay length of $\sim$ 8 km. Of course particle decay is a probabilistic affair. The survival chance of a unstable particle after some time t is governed by an exponential distribution

$$P(t) = e^{\frac{-ct}{\gamma c\tau}} \tag{4.3}$$

The actual decay lengths will therefore also follow an exponential distribution. The high Lorentz boost of the dark photon and parent pion will ensure that the dark photon is likely produced close to the shower core under a small opening angle. In some cases the dark photon will decay after the air shower has already reached its maximum, and most of its energy has dissipated into the atmosphere. The dark photon than decays into standard model particles, with the branching ratios given

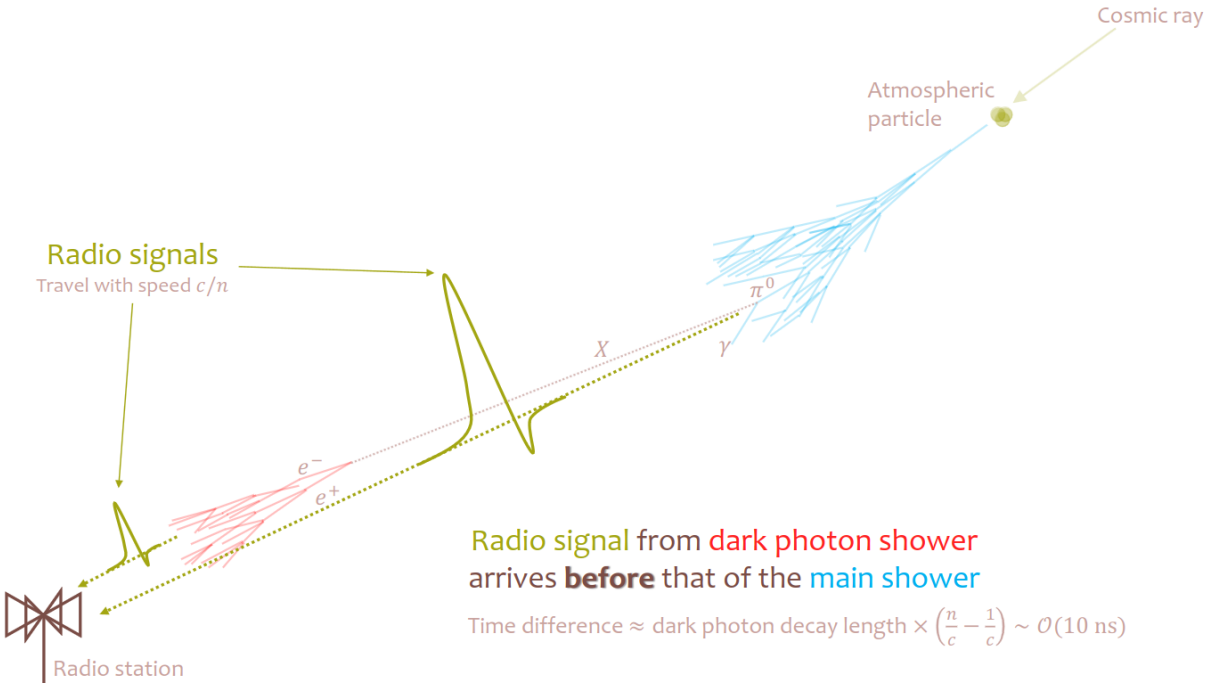

Figure 4.1: A schematic representation of the proposed detection method of dark photons. A dark photon (X) is produced in an air shower, and induces a secondary air shower upon its decay lower in the atmosphere. The arrival time of their respective radio signals are determined by the dark photon decay length and the atmospheric refractive index n. Figure by Anh Phan Vu (Raboud University).

in figure 2.2. These again interact with particles in the atmosphere to produce a secondary air shower, separated from the first shower directly induced by the cosmic ray.

This process could be measured in several ways. Fluorescence detectors could track the longitudinal development of both showers if they are both within their field of view for example. However we are limited by the low flux of high energy cosmic rays, and the low production rate of dark photons in pion decay (see section 4.1). This makes fluorescence detectors, which are relatively expensive, have limited field of view and have an uptime of only 10%, not practical. Particle detectors on the ground might be able to distinguish these events by the lateral distribution of particles on the ground, but this is highly dependant on the shower geometry. If only particles of the secondary shower hit the ground it will have a very small footprint on the Earth's surface, requiring a very dense grid to do observations. If both showers reach the ground it might be possible to distinguish them from ordinary showers through lateral particle distributions. There may for example be an enhanced presence of electromagnetic components close to the shower impact if the secondary shower is a purely electromagnetic cascade induced by a dark photon decaying to an electron-positron pair. However we again run into arguments of flux and surface area. Therefore we choose to look at the radio emission of the air showers as our method of detection. In theory large surfaces areas can be covered with radio antenna arrays, and in radio quiet areas the uptime is close to 100%.

Ideally the radio signal of such an event would contain two distinct peaks in the

antenna response, corresponding to the primary and the secondary shower. The time difference between these peaks is determined by the distance between the two shower maxima in relation to the antenna and the effective refractive index of the atmosphere. The shower particles are all highly relativistic and propagate with approximately light speed through the atmosphere, they are not influenced by the refractive index. The radio signal however is, and propagates with a speed of $\frac{c}{n}$. We define the distance between the two air showers to be the distance between their shower maxima. We then approximate this distance to be the mean decay length of the dark photon. This does not take into account the location where the dark photon is created within the extent of the first shower or the variable index of refraction in the atmosphere. The radio signal of the primary shower has to travel an additional distance $d_{A'}$ compared the radio signal of the secondary shower. The mean difference in arrival times at the antenna becomes:

$$\Delta t \approx d_{A'} \left(\frac{n^*}{c} - \frac{1}{c} \right) \tag{4.4}$$

Using our earlier example for $d_{A'}$ 4.2, and setting the refractive index (averaged over the travelled path in the atmosphere) to $n^* \approx 1.0003$ gives a mean time difference of $\Delta t = 8ns$ between the arrival of the two radio signals. The radio signal of the secondary shower arrives first. The signal strength scales with the shower energy and the distance between the antenna and the location of the radio emission through the inverse-square law. Radio signals are not attenuated by the atmosphere, so the radio signal of the primary shower arrives later, but with a higher intensity. The entire experimental setup described in this section is nicely visualized in figure 4.1.

Our experimental setup is not dissimilar from the principles used in beam dump experiments. Cosmic rays are our beam, the atmosphere provides the 'fixed' target in the form of nitrogen molecules and serves as a dump volume for the primary shower products. The big difference is in the size of our experiment and the detector. The zenith angle of the incoming cosmic rays determines the available length in the atmosphere for the dark photon to decay before hitting the ground, potentially giving us sensitivity to a larger range of mixing parameter than typical beam dump experiments. The high cosmic ray energies lead to large photon fluxes on a per shower basis, however the low flux of high energy cosmic rays may prove to be a problem. The main goal of our simulations will be to try to see if we can achieve a significant measurement given a GRAND sized detector and a reasonable amount of observation time.

4.1 Sensitivity

At the start of this project an analysis was done by Anh Phan Vu on the sensitivity of this experiment, based on the flux of high energy photons produced in inclined proton induced air showers (See figure 4.2). This flux is then converted to a dark photon flux using the branching ratio in equation 4.1. This analysis is based on some assumptions:

- The dark photon is created at the first interaction point.
- The dark photon has an energy of at least 10^{14} eV (left in figure 4.3) or 10^{15} eV (right). This is because it needs to produce an air shower with a measurable

radio signal upon decay. At this point we do not know what lower bound on the dark photon energy needs to be taken. As a consequence this also influences the lowest primary cosmic ray energies we can consider. Since the number of photons scales roughly linear with the primary energy and the cosmic ray spectrum has an index of around -2.7 lower energy air showers contribute more to the total photon flux.

- The dark photon has a decay length between $L_{\min} = 5$ km and $L_{\max} = 80$ km in the Earth's frame. The lower bound is an estimation of the minimal distance needed to resolve two distinct radio signals from the primary and secondary shower. The higher bound is so that the dark photon decays before hitting the ground and the secondary shower has space to develop.

- The following formula is used to determine the number of detected dark photons. This is the formula used in beam dump experiments where the dump volume is placed at a distance L_{min} from the target and ends after L_{max}:

$$N_{\text{signal}} = N_{\text{produced}} \times e^{-\frac{L_{\min}}{d_{A'}}} \left(1 - e^{-\frac{L_{\max}}{d_{A'}}}\right) \tag{4.5}$$

- The detector is assumed to have a perfect detection efficiency.

- There are no background processes.

Figure 4.3 now shows the number of expected events on an area of 3000 km^2 (the surface area of the Pierre Auger observatory) on the parameter plane of the dark photon model for the given assumptions. The yellow line, for example, indicates the contour on the plane for which exactly one detection per year is expected. The greyed out region represents the excluded parameter space shown in figure 2.3. As we can see, under the assumptions mentioned, the experiment has possible sensitivity in the non-excluded gap between the limits placed by the collider and beam dump experiments. This is a strong motivation to start simulating air showers with dark photons included including their radio emissions.

4.2 Background

It is important to consider possible background processes that can give a similar 'double bump' radio signal as described above. We can divide them in background from theories with other long lived particles included and background from standard model processes.

- **Standard model** A fraction of 'normal' air showers shows anomalies in their longitudinal development. An analysis was done in 2011 using the simulation software CONEX [26]. Showers are considered anomalous if a better fit (determined by a χ^2-test) is obtained by the sum of two longitudinal air shower (Gaisser-Hillas) distributions compared to only one. They identify nuclei from either the cosmic ray or the initial target nucleus as the main source of anomalous showers. If not all nucleons participate in the primary interaction they may travel on in small clumps or individual nucleons. They subsequently penetrate deeply into the atmosphere before interacting and causing a secondary

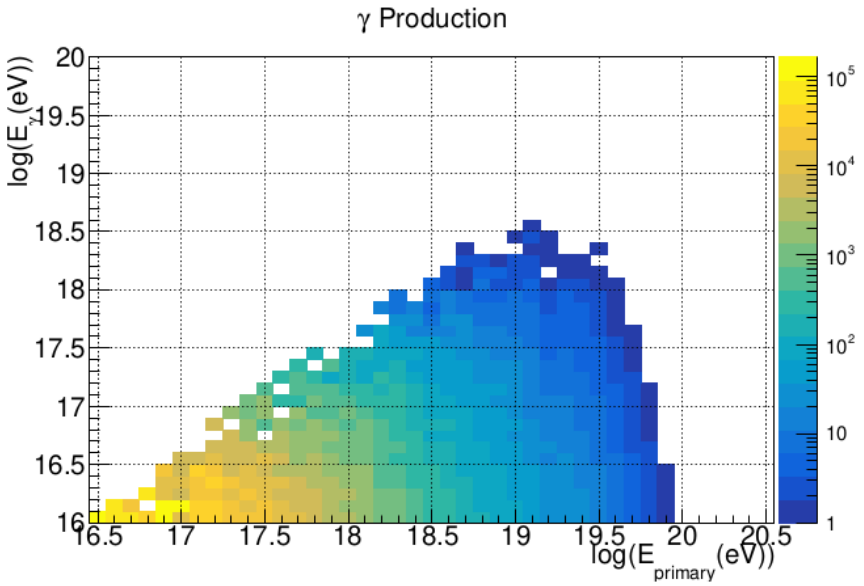

Figure 4.2: Spectrum of high energy photons produced in highly inclined extensive air showers ($\theta_z = 70° - 90°$) on a surface area of 1000 km^2. The primary energy of the cosmic ray is plotted on the horizontal axis. The energy of the produced photons is plotted vertically. Figure by Charles Timmermans (Radboud University).

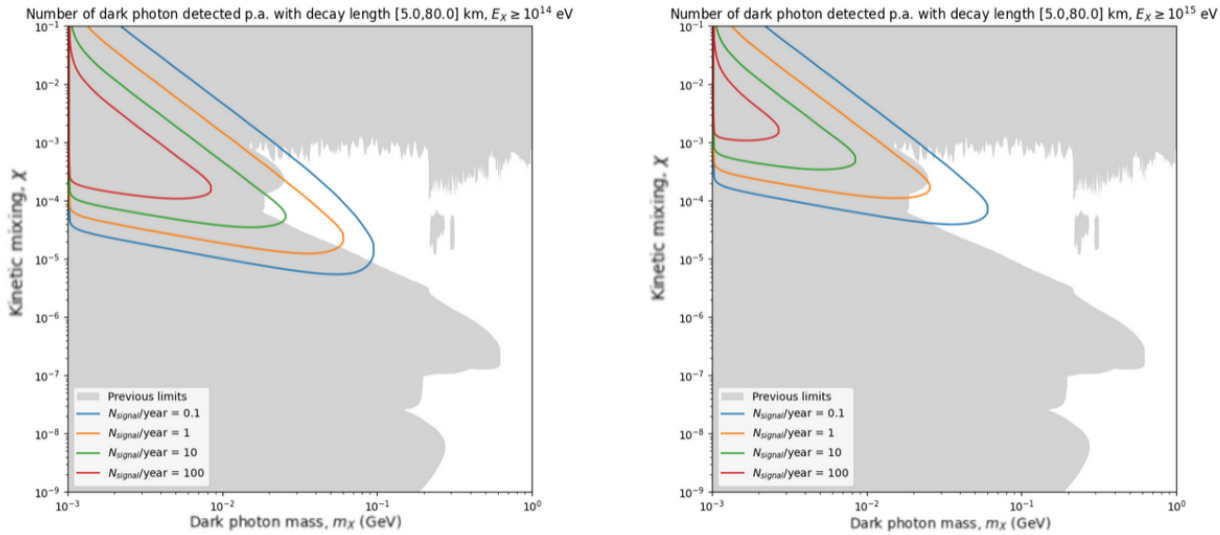

Figure 4.3: Projected sensitivity of the experiment based on the photon flux shown in figure 4.2 and the assumptions explained in the text. The contour lines indicate the number of expected measured events on an area of 3000 km^2 in one year. Assuming the dark photon has at least an energy of $E_{A'} \geq 10^{14}$ eV (Left). $E_{A'} \geq 10^{15}$ eV(Right). Existing limits on the parameter plane are shown in grey. Figures by Anh Phan Vu.

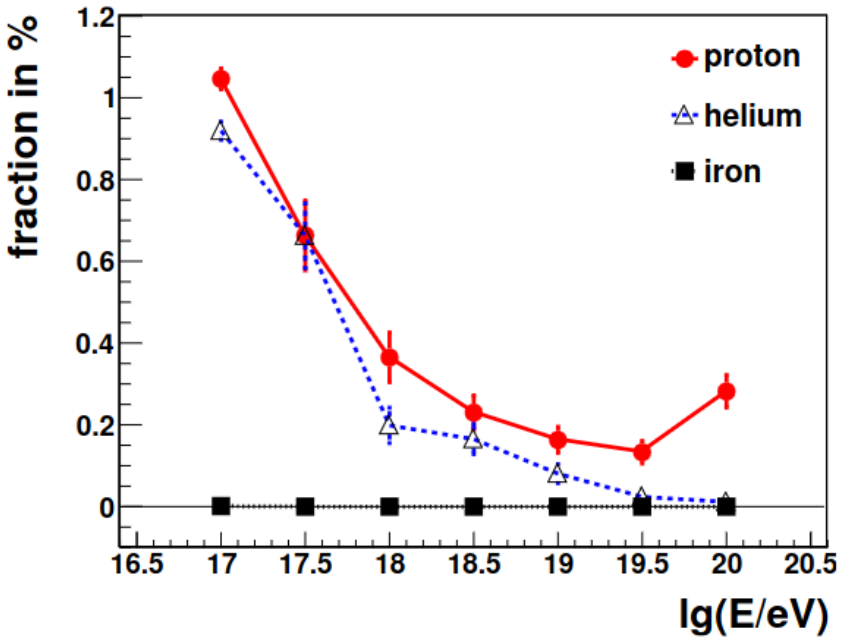

Figure 4.4: The fraction of showers with anomalous longitudinal distributions as a function of primary energy. Based on 10.000 CONEX air shower simulations per cosmic ray mass. The colors indicate the number of photons in each square bin.

shower. Depending on the cosmic ray and target masses the surviving nucleons can carry a large fraction of the primary cosmic ray energy. Based on 10.000 simulations the authors find an anomalous fraction of at most 1% when using SIBYLL as their hadronic interaction model (see figure 4.4). Interestingly iron cosmic rays do not cause anomalous air showers in this analysis. This is because of either the low energy fraction carried by the individual fractured nuclei or the high cross sections of larger clumps of nuclei. They either have a short mean free path length or not enough energy to induce a cascade.

- **Long lived particles** Dark photons are not necessarily the only long lived particles that exist. Other models might for example include Heavy Neutral Leptons (HNL) in addition to dark photons. HNLs also have small coupling to the standard model. If they have similar lifetimes and also produce an electromagnetic cascade upon decaying, like the dark photon, they would cause a similar signal. However the results of this thesis should then be able to be adjusted according to their rate of production in air showers. A very recent paper by Fischer et al. [27] proposes a cosmic ray 'beam dump' experiment to look for HNLs produced by meson decays in air showers. In this case a mountain or the Earth is used as the beam dump volume and respectively a Cherenkov telescope or satellite are suggested as the detectors. In general they consider the HNLs to have much larger lifetimes than we do for the dark photon. Because of these reasons we do not consider HNLs or other possible LLPs in addition to the dark photon.

5. Methods and Results

We can divide the work that was done for this thesis in several parts, each using their own collection of methods and tools. To keep things organized we will discuss the methods, analysis and results of each part separately. This is done in chronological order, to best illustrate the path taken throughout the internship. During the year a lot of time was spend on learning to work [1] with the simulation software and analyzing the output data.

5.1 Where Are the Photons

We start with analyzing the flux and longitudinal distribution of high energy photons in standard model air showers. This work was done before we had implemented dark photons in Aires. We do this for two reasons. First we wanted to do a check on the photon flux shown in figure 4.2. Second, in the previous chapter we made the assumption that the distance between the primary and secondary air shower was the decay length of the dark photon. The dark photon can however be created anywhere in the primary shower where photons are created (with a ratio set by equation 4.1). Having an understanding of the longitudinal distribution of high energy photons then tells us where the dark photons can be created.

To determine the high energy photon flux we simulate proton induced air showers with a zenith angle between 70 and 90 degrees on a detector with a surface area of 1000 km^2. These zenith angles are chosen because we want large radio footprints on the ground. We simulate 2000 showers with primary energies between $E_{\text{primary}} = 10^{16}$ and 10^{20} eV with a flat spectrum (50 simulations per logarithmic primary energy bin). We are only interested in photons produced in the air shower with energies above $E_\gamma = 10^{15}$ eV, so we set the energy threshold of the thinning algorithm to $E_{th} = 10^{14}$ eV. We set the number of observing levels in the atmosphere to 100 and save the tracking information of all photons to the compressed longitudinal data file. A line is written to the data file every time a particle crosses an observation level, so an individual photon can have multiple entries in the file. To ensure we don't overcount the number of produced photons we only count the first entry (corresponding to the first crossing of an observation level) of each individual photon, and discard all subsequent entries for the same photon. We bin the photons according to their own energy and the energy of the original cosmic ray. The bin content is then rescaled with the cosmic ray spectrum (see figure 3.1) and the aperture of the detector. The lowest energy air showers will produce the least high energy photons on a per shower basis. It is the steepness of the cosmic

[1] Using the best learning method known to man: failing a lot and trying again

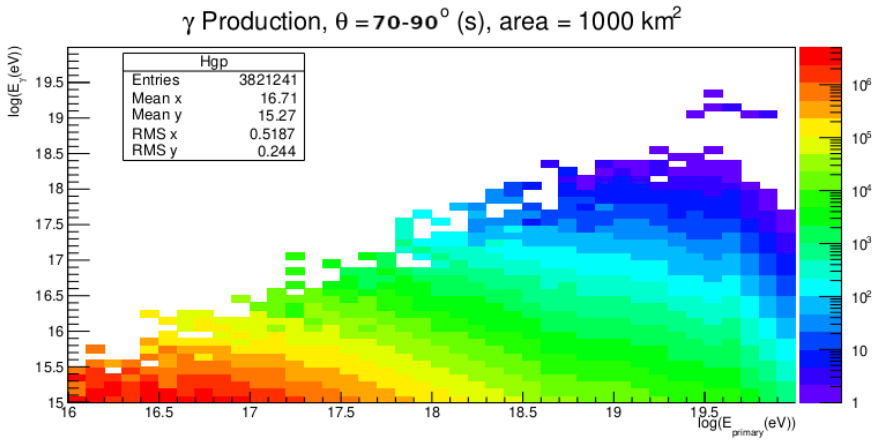

Figure 5.1: High energy photon spectrum for inclined high energy air showers on an area of 1000 km^2. *The primary shower energy is plotted horizontally and the photon energy vertically.*

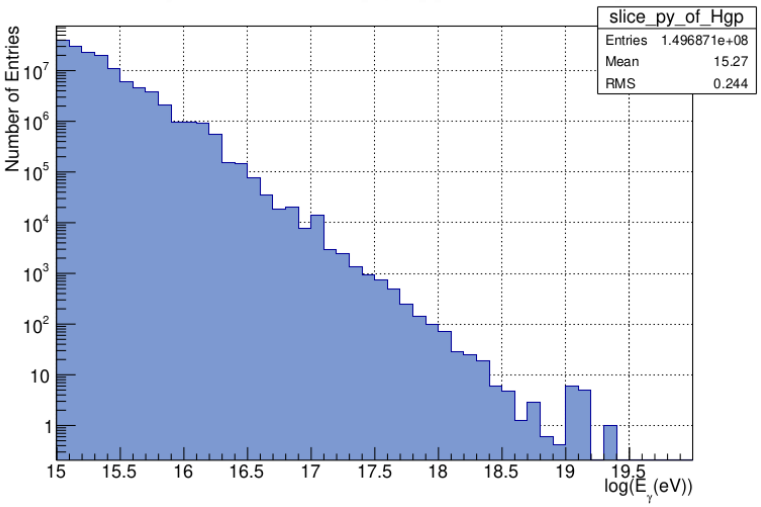

Figure 5.2: Projection of the high energy photon spectrum found in figure 5.1 on the vertical photon energy axis.

ray spectrum that ensures they still contribute the most to the total photon counts. The cosmic ray flux is reduced by a factor of $\mathcal{O}(13)$ over the considered primary energy range. The results can be seen in figure 5.1. Figure 5.2 shows the vertical projection of the spectrum, with photon energy on the horizontal axis and number of photons on the vertical. The spectrum agrees largely with the results found in figure 4.2. This analysis takes slightly lower primary shower energies and photon energies into account. There is a somewhat surprising bump in the projected spectrum at a primary energy of 10^{19} eV. This coincides with the bins in the upper right region of the 2D histogram. The origin is unclear, and is likely a statistical fluctuation or a simulation artifact.

5.1.1 Longitudinal photon distribution

To study the longitudinal photon distribution we simulate 20 proton induced air showers at 10^{18} and 10^{19} and 10^{20} eV each. They have a fixed zenith angle of 60° and we set the thinning energy to $E_{th} = 10^{15}$ eV. We set the number of observing levels to 100. We retrieve the slant depth and energy of the produced photons (with energies of at least 10^{15} eV) from the compressed data file. We plot the number of produced photons (per shower) against the slant depth where the photon is produced, but to get insight in the behaviour of photons at different energies we split the data into several photon energy bins. The results can be found in Appendix A. There are some interesting observations. First, (almost) all high energy photons are created far before the shower maximum has been reached. The shower maxima are in the range of $750 - 880$ g/cm^2. Only for the 10^{20} eV showers there are some photons created after the maximum has been reached. Second, we can see that the maximum of the photon distributions start in the $100 - 300$ g/cm^2 range for the lower energy photons. It moves to the left when going higher in photon energies, until eventually the maximum lies in the first bin. From this we can confirm that most dark photons capable of starting a secondary shower upon their decay will be produced early in the development of the primary shower. Only the highest energy air showers will occasionally produce a high energy dark photon near their shower maximum, which can lead to higher than average time differences between the radio emission of the two showers.

5.2 Implementation

To simulate dark photons in air showers we need to modify existing software to include our model. The modifications were done by Charles Timmermans. Since this research is largely exploratory in nature we keep the implementation simple. We start with a basic installation of AIRES 19.04.08 and make the following model choices and implement these features:

- Dark photons are only produced in neutral pion decays. We add the processes $\pi^0 \to \gamma A'$ and $\pi^0 \to A'A'$ to the possible pion decay channels in AIRES and update the branching ratios according to equation 4.1. This choice limits the dark photon masses we can study to $m_{A'} \leq m_{\pi^0} \approx 135$ MeV.

- Dark photons only decay to electron-positron pairs. This sets a lower mass limit on the dark photons of $m_{A'} \geq 2m_{e^-} \approx 1.02$ MeV.

- To compensate for the low production rates of dark photons a 'production boost' feature is implemented. This input parameter linearly increases the number of dark photons produced by modifying the neutral pion decay branching ratios. It does not modify the dark photon decay. This feature allows us to decrease the number of simulations we have to run, which is important since simulating an individual air showers with their radio emissions can take more than 15 minutes. We make the assumption that the number of double bump radio signals also scales linearly with the production boost. We often take care to keep $\epsilon^2 *$ production boost ≤ 0.001, to limit any potential side effects

caused by a large number of dark photons in the air shower. The possible side effects have not been studied, but the slow decay of dark photons compared to normal photons might influence the longitudinal shower development. We could also start seeing even more exotic signals like triple bumps, with two separate dark photons starting large additional air showers.

- The mass, mixing parameter and production boost are controlled with the following AIRES input directives: DGMass, DGEpsilon and DGBoost.

- In the following simulations we generally set $m_{A'} = 50$ MeV, $\epsilon = 10^{-4}$ and production boost $= 10^6$. If no other values are specified in a figure these settings were used.

Several tests were done to see if the dark photon production and decay behaved as expected. In figure 5.3 we show the results of simulating 1000 air showers with dark photons enabled. The plots show the energy and decay length spectrum of dark photons (with energies above 10^{13} eV) in 10^{19} eV air showers. We use a high production boost for better statistics, this is not divided out in these plots. Only dark photons that actually decay in the atmosphere are shown. Note that a portion of the dark photons actually hit the ground before decaying. We have confirmed that dark photons are produced in the modified AIRES installation, and some indeed decay after long distances. For the peak in the dark photon energy distribution at 10^{14} eV we find a mean decay length of 0.32 km. Clearly the mean lifetime increases for higher energy dark photons, leading to larger decay lengths. Appendix B contains the 2d-histogram plots for a lower dark photon mass and several primary energies and mixing parameters.

We can also plot the longitudinal development of the air shower to see if we actually see a secondary shower being formed. In figure 5.4 we see two examples where a clear secondary shower is formed. This strongly deviates from the average shower profile seen in figure 3.4. Despite the high boost factor only few showers show this behaviour. We could write an algorithm to select only the showers that show two bumps, for example by using the method used to distinguish anomalous showers described in the previous chapter. But in our experiment we only collect data from radio antennas, so we will attempt to discriminate the double bump showers only on their radio emission.

As a final check we will calculate the dark photon spectrum for two different mixing parameters. The same methods are used as for the high energy photon spectrum in figure 5.1. We take the aperture of a 1000 square kilometer detector and the cosmic ray flux into account. A production boost was applied to these simulations, the results shown are the number of dark photons divided by the used production boost. Over a year we find the shown spectra for dark photons with a mass of 50 MeV in figures 5.5 and 5.6. For a mixing parameter of $\epsilon = 10^{-4}$ we expect to see around one high energy dark photon in a year. If we go to $\epsilon = 10^{-3}$ we see that the total number increases roughly quadratically to 135, which we expect because of equation 4.1.

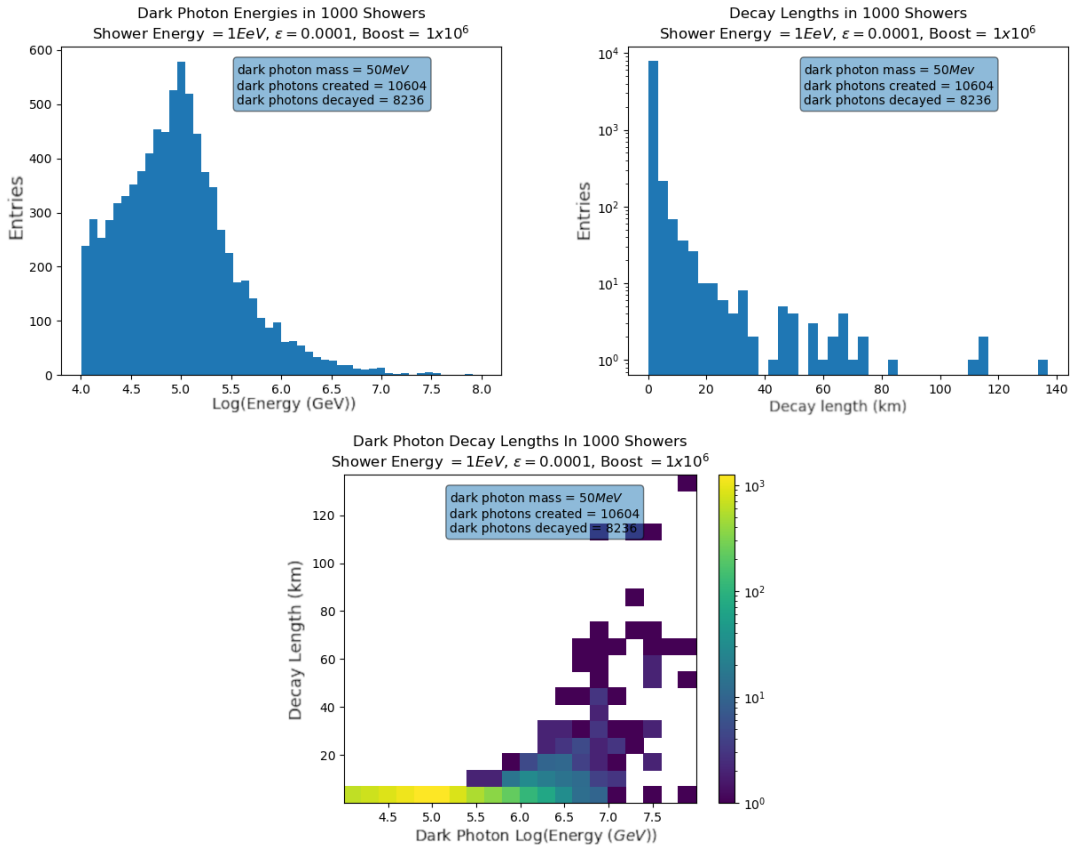

Figure 5.3: Energy and decay length histograms for dark photons produced in 1000 EeV air showers. The dark photon production is boosted by a factor of 10^6. $\theta_z = 80°$.

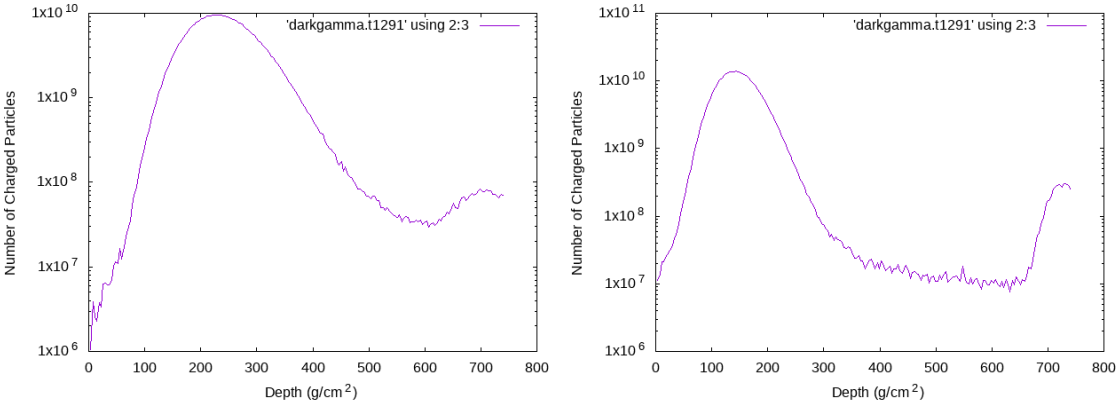

Figure 5.4: longitudinal development of two inclined 'double bump' anomalous air showers. Only the charged particles are counted, since these account for the radio emission of the air shower. The horizontal axis shows the vertical depth. $E_{primary} = 10^{19}$ eV, $m_{A'} = 50$ MeV, $\epsilon = 10^{-4}$, $\theta_z = 80°$, production boost $= 10^6$.

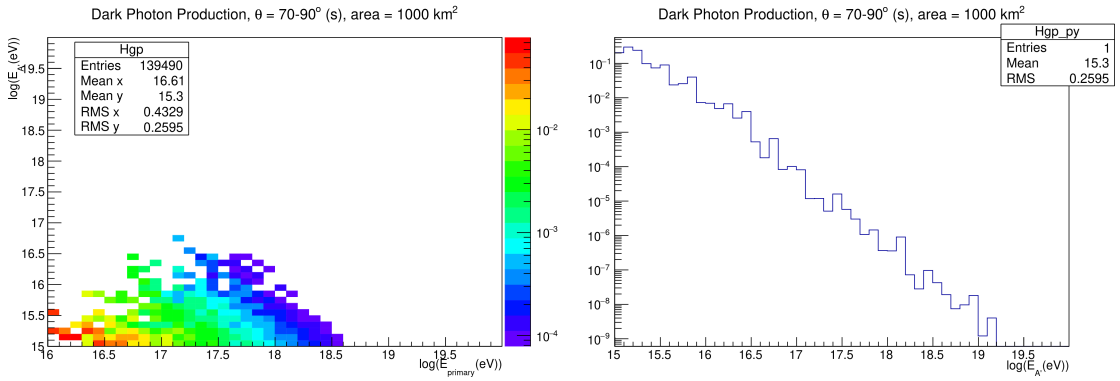

Figure 5.5: Dark photon energy spectrum from modified AIRES simulations. $m_{A'} = 50$ MeV, $\epsilon = 10^{-4}$. Dark photons that decay within 5 km of the primary vertex are not counted. Left: the spectrum as a function of shower energy and dark photon energy. Note: the number after Entries in the text box does not correspond to the total number of dark photons produced. Right: The spectrum projected on the dark photon energy axis.

5.3 Listening To The Radio

We simulate the time domain radio response of the showers with ZHAireS. We only simulate the response of a single antenna, which we have virtually placed in Lenghu, China. ZHAireS automatically takes the local geomagnetic field into account. It is a highly elevated region, and we define the ground at 2700 m above sea level. The software gives the vector components of the local electric field at the antenna as its output. We convert this to the absolute value of the electric field $|E|$. At this point our goal is to develop an algorithm that finds the anomalous double bump showers based on this output. The algorithm used is as follows:

- Record all peaks in the electric field strength that reach above some threshold value E_{th}.
- If the number of peaks is less than two (within 300 ns of the first radio signal recorded) the simulation is discarded. Else proceed.

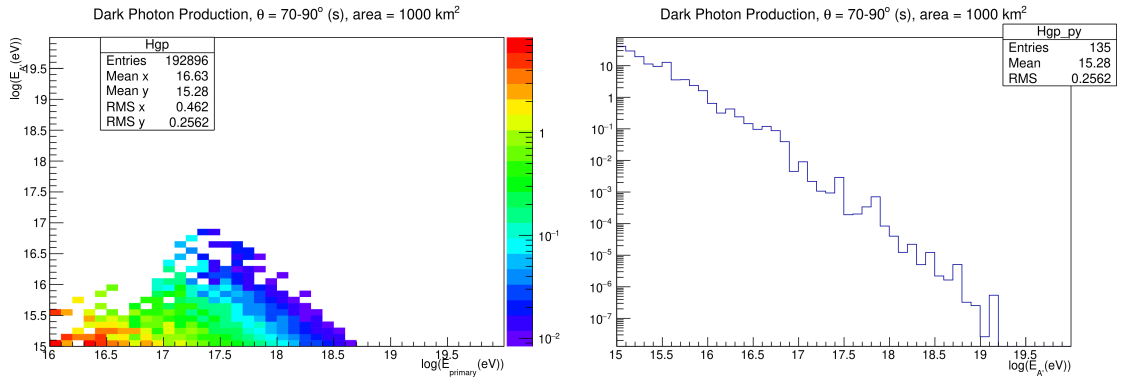

Figure 5.6: Dark photon energy spectrum from modified AIRES simulations. $m_{A'} = 50$ MeV, $\epsilon = 10^{-3}$. Dark photons that decay within 5 km of the primary vertex are not counted. Left: the spectrum as a function of shower energy and dark photon energy. Note: the number after Entries in the text box does not correspond to the total number of dark photons produced. Right: The spectrum projected on the dark photon energy axis.

- Find the time difference between the two highest peaks in the signal, and calculate the ratio between their respective $|E|$ values.
- If the time difference is larger than $\Delta t_{\min}$ and the peak ratio exceeds the threshold values $R_{\min}$ and the highest peak takes place after the second highest peak the air shower is marked as a double bump signal event.

With this algorithm we try to select events based on the known physics of the system; We expect two radio peaks corresponding to the two air showers with some time delay between their arrival times. The primary shower carries more energy and develops further away from the antenna, so has a higher intensity but arrives later. E_{th} is introduced to exclude peaks in the radio response due to simulation noise. We have set the thinning energy of AIRES to 10^{-6} relative to the primary shower energy in the radio emission simulations. After some tests this seemed to give a reasonable balance between computing times and fluctuations in the longitudinal development and radio emissions. The dark photons considered in the calculated flux will always fall above this energy threshold, and so will not be subject to any thinning.

This algorithm has been successfully employed on sets of air shower simulations with dark photons enabled. In fact the air shower simulations seen in figure 5.4 were found in a set of 15.000 simulations of 10^{19} eV highly inclined ($\theta_z = 70° - 90°$) air showers. The radio signals corresponding to these showers are shown in figure 5.7 Using $|E|_{th} = 10^{-3}$ V/m, $\Delta t_{\min} = 10$ ns and $R_{\min} = 0.1$ we in fact find 42 double bump signal events. In a later section we will compare the number of simulations to the number of expected air showers at a GRAND sized detector. This is a nice result, but we need to be a little bit careful. Not all simulations selected this way will clearly show two peaks in their longitudinal particle distributions. We also see that showers with a particularly wide longitudinal development have a higher tendency to be selected as signal events. A possible explanation is that the change in particle current (i.e. increasing and decreasing charged particle numbers) happen further apart from each other in the atmosphere than normal, and thus the radio signal induced by these changes in current may arrive at the antenna at different

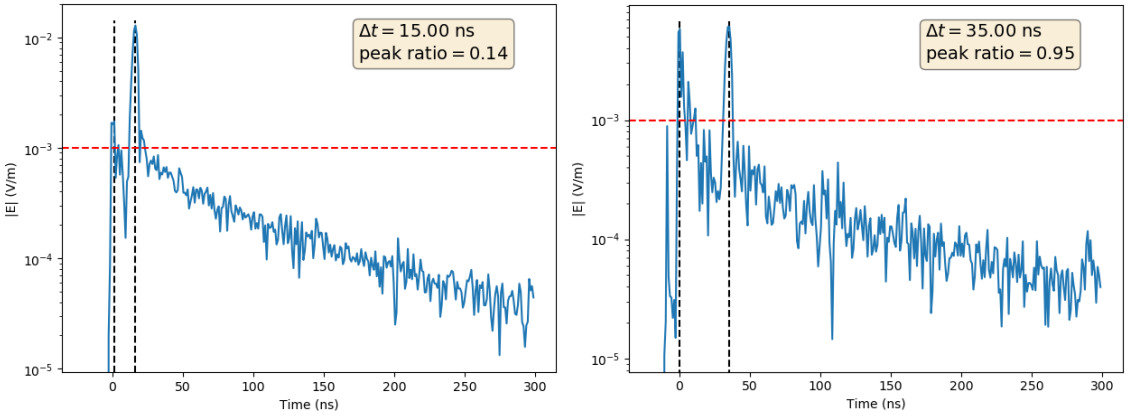

Figure 5.7: The radio response corresponding to the air shower simulations shown in figure 5.4. The horizontal red line represents the threshold value $|E|_{th}$.

times. An example of both these cases, from the same data set as before are shown in figure 5.8. Certainly in the top shower it is clear that a dark photon has not induced a secondary shower of any significant size. For the bottom shower this is not as clear, it might be that the two air showers simply overlap to form this distribution. We are not able to confirm this from our simulation data. If these events are in fact false positives we will also see them in our 'standard model air showers' without dark photons. So we will also simulate many standard model air showers as a background. If any standard model air showers are marked as signal events for some set of selection criteria we can take this into account when determining the significance of our dark photon signal.

We have also (anecdotally) observed that the radio signal of the secondary shower seems to be much stronger relative to the primary shower when it hits the ground during its development. This has not been studied further, but it might be caused by the 'sudden death' mechanism described in reference [28]. Here it is stated that the sudden deceleration of electrons and positrons created in a high energy air shower upon hitting the Earth can cause a radio signal with a strength in the order of 15 μ V/m. This is way lower than the radio signal strength seen in our examples, but the pulse was calculated was from a normal vertical 10^{18} eV air shower. The increased energy and number of charged particles at the ground due to the secondary shower could potentially cause a much stronger sudden death radio pulse. The pulse might however be too low in frequency for air shower antennas to catch. The sudden death pulse is coherent up to only 20 MHz, and air shower antennas generally operate above 30 MHz.

5.4 Any Significance?

Now that we have set up the algorithm to analyze our simulations we want to perform a statistical analysis. We investigate if there is a signal above a background of standard model air showers, and what the significance of this signal is. Our method is as follows:

- We simulated large data sets of showers with and without dark photons. Be-

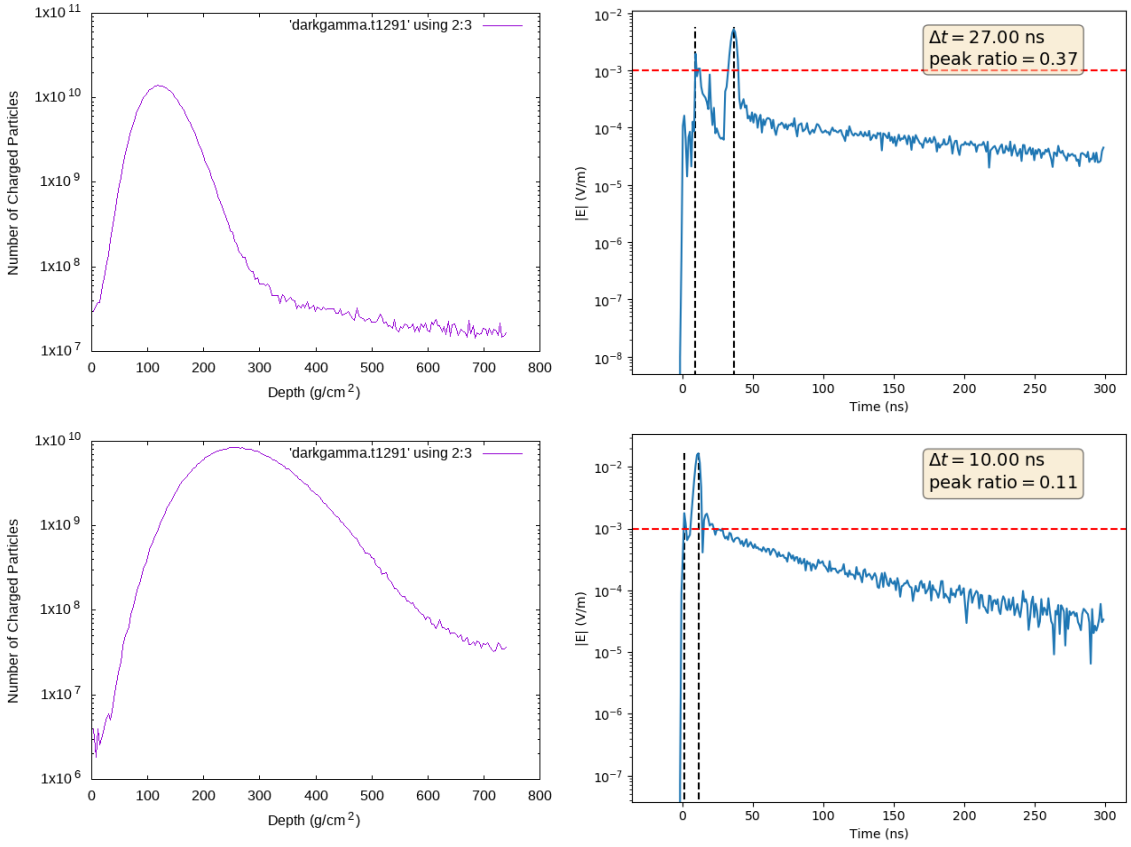

Figure 5.8: Examples of questionable selected signal events and their radio signals. Top: no interesting features can be seen in the longitudinal shower development, yet the radio signal meet our signal criteria. Bottom: This shower has a wide distribution, which seems to increase the chances of meeting the algorithm criteria.

cause we need to simulate large amounts of air showers we cannot make data sets for many points in the dark photon parameter plane. We have made data sets of dark photon implemented air showers with energies of 10^{16}, $10^{17.5}$ and 10^{19} eV. We again use dark photons with a mass of $m_{A'} = 50$ MeV, $\epsilon = 10^{-4}$ and a production boost of 10^6. After that we also made a set of 10^{16} eV showers with $\epsilon = 10^{-3}$ (decreasing the production boost by two orders of magnitude at the same time). For all three shower energies we have also performed simulations with a standard AIRES installation to determine the standard model background.

- We analyze the sets with our double bump selection algorithm. To find the optimal selection criteria we iterated over a range of values for $|E|_{th}$, $\Delta t_{\min}$ and $R_{\min}$.

- We define a significance measure based on the size of the simulated dark photon and standard model data sets (n_{dp}, n_{sm}), the selected signal events in both sets $(s_{dp},\ s_{sm})$ and the production boost factor:

$$\sigma = \frac{(s_{dp} - \frac{n_{dp}}{n_{sm}} s_{sm})/\text{boost}}{\sqrt{s_{dp} + (\text{boost} - 1)\frac{n_{dp}}{n_{sm}} s_{sm})/\text{boost}}} \tag{5.1}$$

This slightly strange looking definition is needed because the dark photon implemented shower simulations are still undergoing all the same processes as the standard model showers, and therefore will also have possible background signals purely from standard model processes. So the dark photon signal is recovered by essentially subtracting s_{sm} from s_{dp}, while taking into account the difference in size of the data sets and the dark photon production boost (which effectively multiplies the size of the dark photon data sets. Say we simulated 10.000 dark photon showers with a production boost of 10^6, This is treated the same as if we simulated 10^{10} air showers without a production boost). If there are no selected events in the standard model shower data set for given selection criteria the formula simplifies to $\sigma = \sqrt{s_{dp}/\text{boost}}$.

We plot the number of selected signal events in the dark photon showers, in the standard model showers and the resulting significance in heat maps. These are not histograms, the colors do not indicate the number of events within a certain bin. The colors indicate the number of selected events that pass that specific combination of minimal time difference Δt_{min} and minimal peak ratio R_{min} criteria. The more stringent the criteria become the fewer air showers will be marked as signal events by the algorithm. We do not show the results for all values of $|E|_{th}$ considered, we only show the threshold resulting in the highest possible significance for each choice of shower energy and mixing parameter (and in case of ties we default to the highest threshold value.)

We make the following observations about the results, which are shown in figures 5.9 through 5.12 for the studied primary energies and mixing ratios:

- We do not find very high significance numbers (generally in particle physics a discovery is claimed at 5σ). Essentially this means the number of dark photon showers we have simulated was not enough to find a significant signal. The number of simulations done should be increased if we want to find higher significance numbers. In an experiment this would mean we need to measure longer or have a larger detector to measure more showers and find a larger signal. The number of showers simulated can be converted to a detection time by considering the cosmic ray flux on a detector with some area. If we take the signal found in figure 5.12 (7 signal events in effectively 30.000 $\times$ production boost $= 3 \times 10^8$ showers, no background from the standard model) and consider the flux of 10^{16} eV cosmic rays in figure 3.1 (around 1 year^{-1}m^{-2}) we find that in a year we should see about 4667 double bump events in a total of $200 * 10^9$ air showers with a primary energy of 10^{16} eV at a GRAND sized detector for the chosen dark photon mass and mixing parameter.

- Where there is a standard model background it almost fully suppresses the signal significance. In fact the when looking at the shape of the plots the significance plot covers exactly the area where only air showers with dark photons have events selected. You can fit the selected standard model showers plot in the significance plots as a puzzle piece. The significance is not exactly zero in the standard model background region, but is suppressed by two to four orders of magnitude.

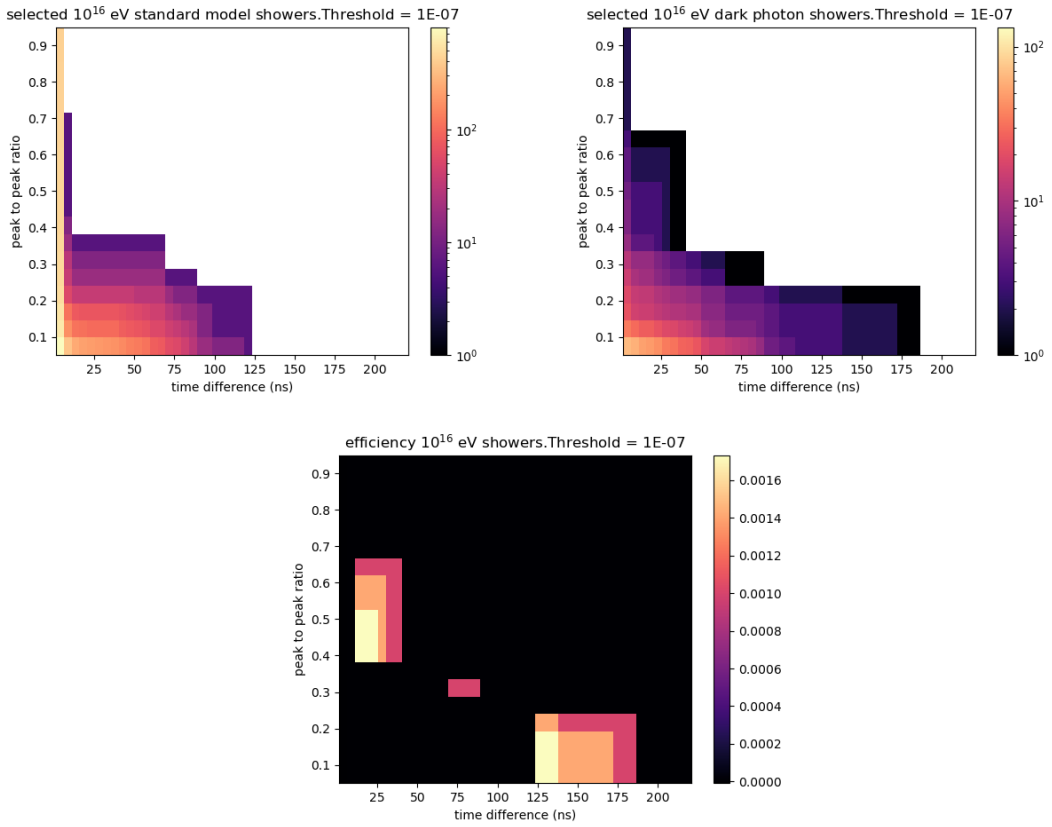

Figure 5.9: Double bump signal analysis of dark photons in 10^{16} eV inclined air showers. based on 5000 dark photon air shower simulations and 5000 standard model shower simulations. $m_{A'} = 50$ MeV, $\epsilon = 10^{-4}$, production boost = 10^6. The highest significance reached is 0.0017, in both a region of low and high minimal time difference. In these regions there are 3 signals selected in the dark photon shower simulations and 0 in the standard model simulations.

- We see that for the showers with $\epsilon = 10^{-4}$ the best results are found for the 10^{19} eV showers. This is in itself not surprising, since simply more dark photons are produced in higher energy air showers. Interestingly the background from the standard model showers does not go above a minimum peak to peak ratio of 0.2. This is likely because the main radio pulse of the primary shower has a higher intensity compared to the lower energy air showers. Any simulation noise or background from standard model processes will therefore have a lower relative height compared to the primary radio pulse.

- The significance of the 10^{16} and $10^{17.5}$ eV air showers are lower than that of the 10^{19} eV showers (but equal to each other), but only by roughly a factor of three. So though we expect more measurable double bump events on a per shower basis for higher energy showers, the sheer difference in cosmic ray flux for these air shower energies means the 10^{16} eV air showers should contribute by far the most to the total signal count. This is also the reason why we chose to simulate a second set of 10^{16} eV air showers, this time with a mixing parameter of 10^{-3} and production boost of 10^4. This turns out to be a more point in the dark photon parameter plane where our experiment would be more sensitive, and the significance increases by a factor 15 compared to the

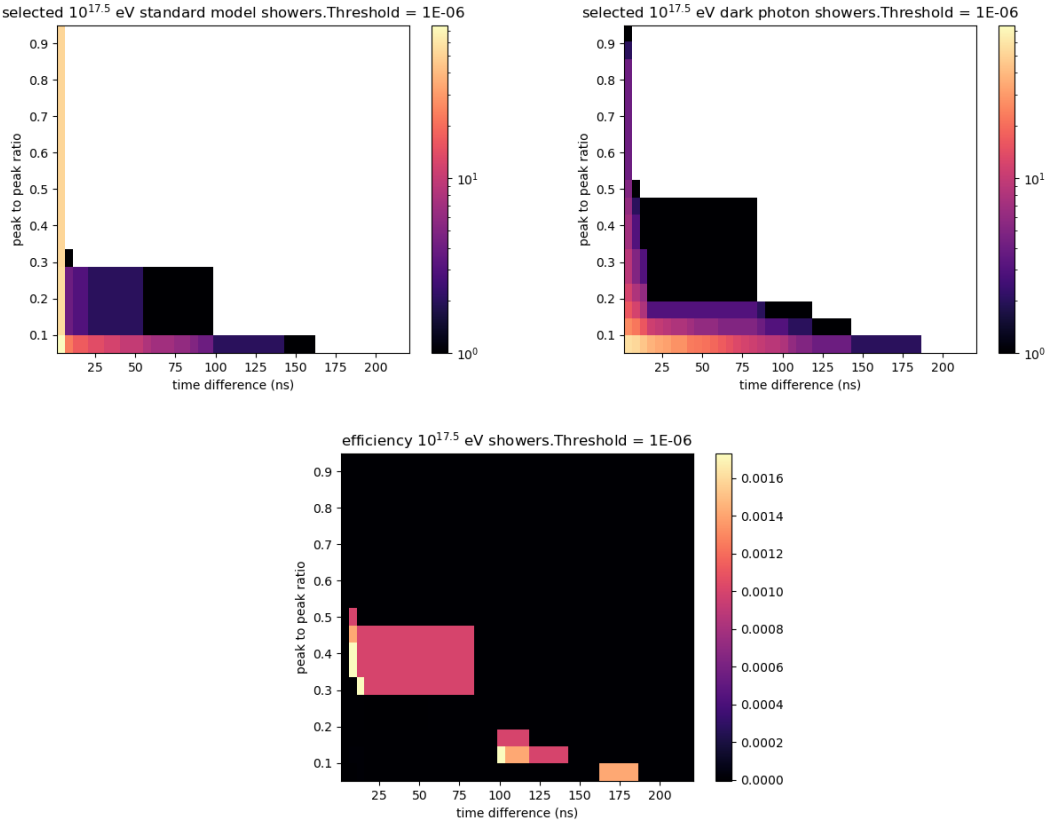

Figure 5.10: Double bump signal analysis of dark photons in $10^{17.5}$ eV inclined air showers. based on 5000 dark photon air shower simulations and 5000 standard model shower simulations. $m_{A'} = 50$ MeV, $\epsilon = 10^{-4}$, production boost $= 10^6$. The highest significance reached is again 0.0017, in both a region of low and high minimal time difference. In these regions there are 3 signals selected in the dark photon shower simulations and 0 in the standard model simulations.

10^{16} eV air showers with $\epsilon = 10^{-4}$.

- In the significance/efficiency plots we generally see two regions where the significance reaches its highest point. One for low minimum time differences and high minimum peak to peak ratios, and vice versa. The existence of the low time difference region is slightly surprising, since it implies that we may see some effect from very high energy dark photons decaying relatively quickly. These regions in all cases have the same number of selected dark photon showers, but this could be a coincidence. It is possible that the selected showers in both regions do not overlap, in which case we could possibly combine them to get a stronger total signal. We checked this for the latest simulations we did, the 10^{16} eV air showers with $\epsilon = 10^{-3}$. Both regions correspond to 7 selected dark photon showers and zero selected standard model showers. The selected dark photon showers in the regions share no overlap, for a total of 14 selected air showers outside the standard model background region. However we also have to place a critical note. Of those 14 selected air showers only 4 clearly show a secondary shower developing in the longitudinal shower distribution. One of these is in the low minimum time difference area, the other three in the high minimum time difference area. This would correspond to a signifi-

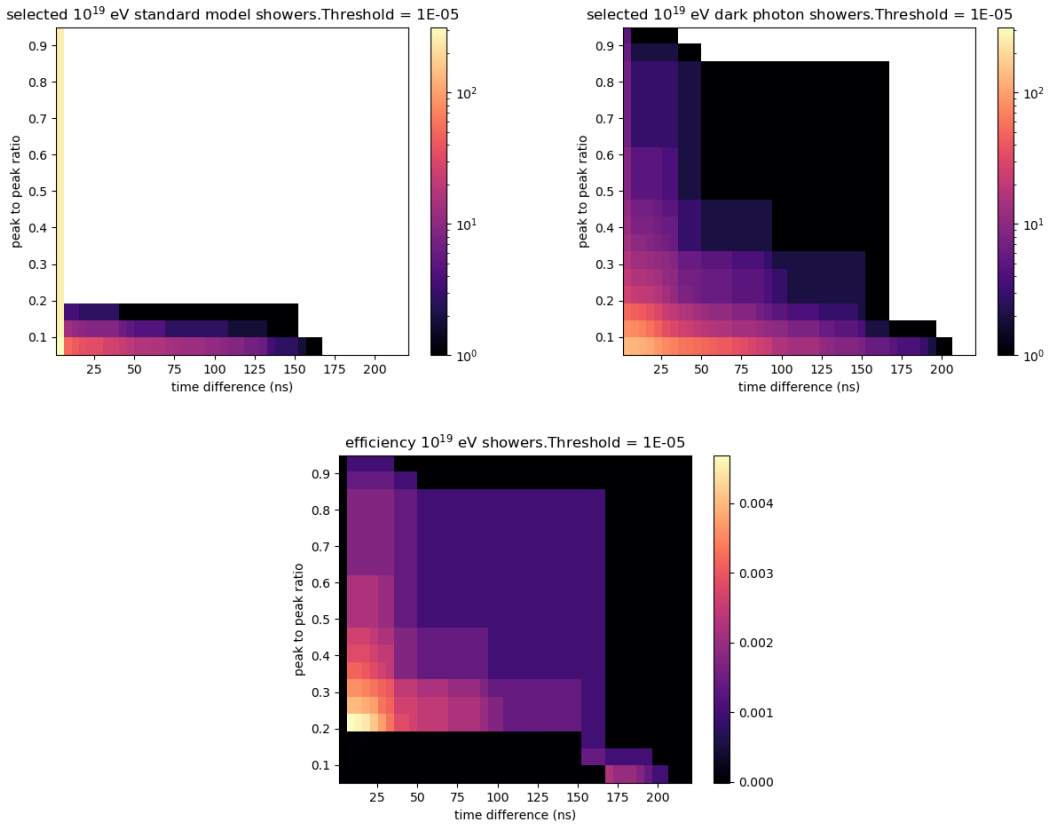

Figure 5.11: Double bump signal analysis of dark photons in 10^{19} *eV inclined air showers. Based on 15000 dark photon air shower simulations and 15000 standard model shower simulations.* $m_{A'} = 50$ *MeV,* $\epsilon = 10^{-4}$*, production boost* $= 10^6$*. The highest significance reached is now 0.0047. In this single region there are 22 signals selected in the dark photon shower simulations and 0 in the standard model simulations.*

cance of $\sigma = 0.02$. Multiplying the number of signal events (four) with the ratio of expected showers in a year at a GRAND sized detector to the number of simulated air showers times the production boost factor used we recover a significance of $\sigma = 0.516$. If we only take showers with a primary energy of 10^{16} eV into account this means it would take around 94 years to reach $\sigma = 5$ at GRAND. Of course including the higher energy air showers would decrease the number of years needed. Without doing more simulations it is hard to say if we should consider the remaining ten showers as a signal or not. They are outside of the standard model shower background, so even though the longitudinal shower profile does not have the expected form it may still be a signal of a dark photon decaying. At this point we cannot say, and it is safest to assume to not consider them as signal events.

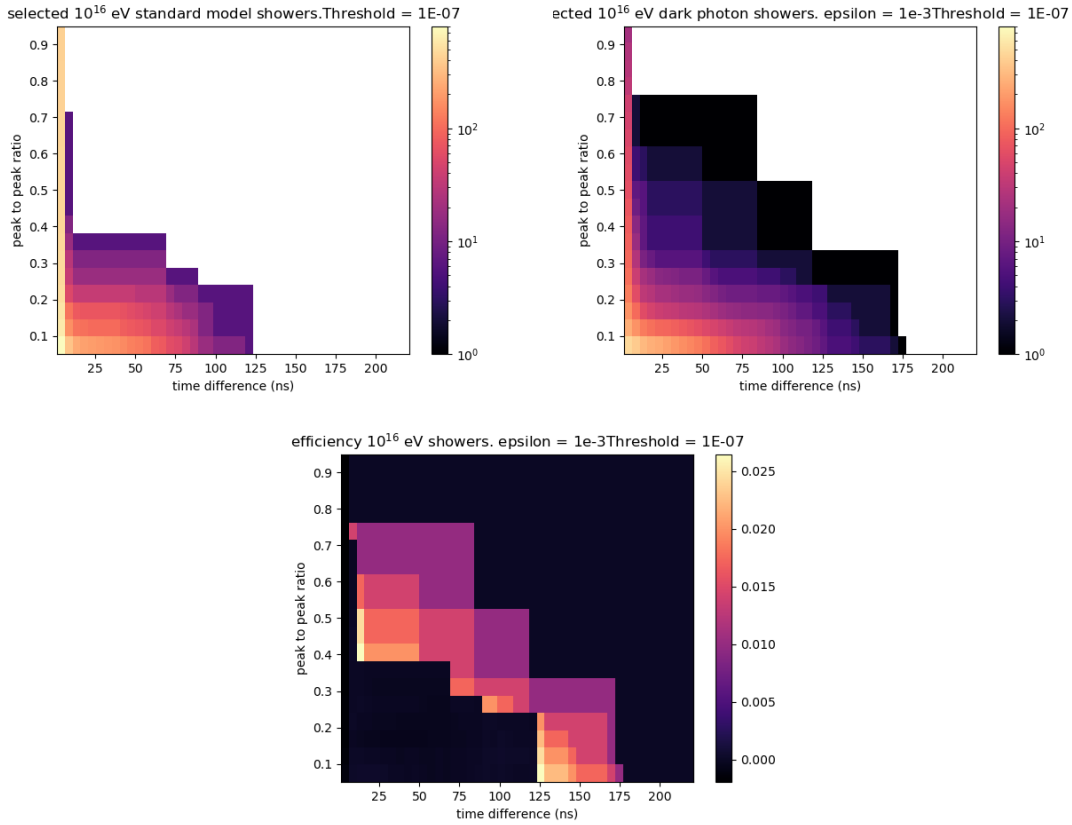

Figure 5.12: Double bump signal analysis of dark photons in 10^{16} eV inclined air showers, but this time for a higher value of the dark photon mixing parameter. Based on 30000 dark photon air shower simulations and 5000 standard model shower simulations. $m_{A'} = 50$ MeV, $\epsilon = 10^{-3}$, production boost = 10^4. The highest significance reached is now 0.0265. again there are two high significance regions, with 7 signals selected in the dark photon shower simulations and 0 in the standard model simulations in both regions.

6. Conclusion

We arrive at the end of this project at somewhat awkward time. A lot of work has already been done. We have combined the theories of extensive air showers and dark photons and used that to propose an exciting novel way to search for new physics. A simple version of the dark photon phenomenology has been implemented in air shower simulation software. Many tests have been done to see if the implementation worked, and it seems to work very well. We have seen exactly the double shower profiles we wanted to see in our simulations, one from the incoming cosmic ray and one from a dark photon decaying later on in the atmosphere. And in fact we see them in the radio signals as well, with time differences between the radio peaks that are in the right theoretical range. The infrastructure to simulate large amounts of air showers, and to analyze them, has been build piece by piece over the last year. And we have made a start with those simulations, and have found that our dark photon simulations in fact produce signatures in the radio signal that are not found in standard model background air shower radio emissions. We have shown there is a small signal above the standard model background, and that air showers in the 10^{16} eV range will contribute the most to this signal compared to higher energy air showers. But this is really only a start. Only two points in the dark photon parameter plane have been studied, and those only for a few air shower energies. To achieve a more complete picture simulations should be done for the full high energy air shower spectrum, and over the entire relevant area in the dark photon parameter plane.

This is not meant to be negative, in fact I hope anyone who has read this thesis sees that it is worthwhile to continue this exploration. It might take a lot of work and cpu time, but there is a real possibility to probe the dark photon parameter space. We will end this thesis with recommendations for continued research and some tangential lines of inquiry that could be explored further.

- I recommend that any direct follow up on this thesis split their research into two parts. First we need a better understanding of the influence of a high energy dark photon in the air shower on the radio signal. Although our simple selection algorithm does produce results I believe a better understanding of the shape of the possible radio pulses can lead to a much better algorithm. For example we have seen that dark photon air showers without a clear second peak in the longitudinal distribution can still produce a double bump radio signal that is not replicated in our standard model background. We have also seen that air showers with a wide distribution tend to show two peaks in the radio signal with short time differences.
  I suggest that the special primary routine in AIRES is used to consistently

simulate air showers with a decaying high energy dark photon by manually adding a electron-positron pair along the shower axis. In this way the decay length and energies can be chosen. In this way we do not need to rely on large sets of simulated showers where most simulations will not have a secondary air shower. It might also be interesting to use this setup to see if there is a strong 'sudden death on ground' effect from the secondary air shower on the radio signal, as described in reference [28].
After this has been done a statistical analysis can be done in the same vein as the one done in the previous chapter, but using an improved selection algorithm with a better understanding of the possible radio signal shapes. Also one can look into ways to improve the simulation time per shower and radio signal, perhaps even by using different simulation software.

- We have given arguments why a radio antenna array is a good choice of detector, but have only looked at the response of a single antenna. A full grid could be simulated to study the radio footprint on the ground in detail. It could also be interesting to analyze the response from fluorescence detectors and surface particle detectors. The secondary shower might have a measurable influence on the lateral particle distribution on the ground.

- Inspiration can be taken from the cosmic ray beam dump experiment described in [27]. In this case a dark photon is produced in an air shower that is aimed at a mountain. It travels through the mountain and decays after it has passed. Radio antennas on both sides of the mountain would pick up a signal with only a small time delay between them. This would be an even less frequent event than the one we describe, but eliminates the need to look for two close radio pulses in one antenna readout.

- If this research would be taken up by experimental groups like GRAND, the practical implementation of this research should be studied. The double bump events must be taken into account when, for example, designing the trigger algorithms. The bumps happen within a short time from each other, and the radio signal of the secondary shower is small compared to that of the primary. How can you make sure the small signal is not discarded at the trigger level and how do you do this with limited computing resources?

Bibliography

[1] Katherine Garrett and Gintaras Duda. Dark matter: A primer. *Advances in Astronomy*, 2011:1–22, 2011.

[2] Bob Holdom. Two U(1)'s and Epsilon Charge Shifts. *Phys. Lett. B*, 166:196–198, 1986.

[3] Alessandra Filippi and M. De Napoli. Searching in the dark: the hunt for the dark photon. *Reviews in Physics*, 5:100042, nov 2020.

[4] Thomas K. Gaisser, Ralph Engel, and Elisa Resconi. *Cosmic Rays and Particle Physics*. Cambridge University Press, 2 edition, 2016.

[5] D. J. Griffiths. *Introduction to elementary particles; 2nd rev. version*. Physics textbook. Wiley, New York, NY, 2008.

[6] M. E. Peskin and D. V. Schroeder. *An introduction to quantum field theory*. Westview, Boulder, CO, 1995.

[7] Jim Alexander et al. Dark sectors 2016 workshop: Community report, 2016.

[8] Bart Steeman. Bachelor's thesis: Sterile neutrinos dark matter. 2021.

[9] Patrick Foldenauer. Dark sectors from the hidden photon perspective, 2019.

[10] Marco Fabbrichesi, Emidio Gabrielli, and Gaia Lanfranchi. *The Physics of the Dark Photon*. Springer International Publishing, 2021.

[11] Philip Ilten, Yotam Soreq, Mike Williams, and Wei Xue. Serendipity in dark photon searches. *Journal of High Energy Physics*, 2018(6), jun 2018.

[12] Jia Liu, Neal Weiner, and Wei Xue. Signals of a light dark force in the galactic center. *Journal of High Energy Physics*, 2015(8), aug 2015.

[13] Martin Bauer, Patrick Foldenauer, and Joerg Jaeckel. Hunting all the hidden photons. *Journal of High Energy Physics*, 2018(7), jul 2018.

[14] Danilo Zavrtanik. Ultra high-energy cosmic rays - experimental status. *Journal of Physics G: Nuclear and Particle Physics*, 27:1597, 06 2001.

[15] Todor Stanev. Cosmic Rays and Extensive Air Showers. 2010.

[16] Daniel Gomez Toro. *Temporal Filtering with Soft Error Detection and Correction Technique for Radiation Hardening Based on a C-element and BICS*. PhD thesis, 12 2014.

[17] Dariusz Góra and. The pierre auger observatory: Review of latest results and perspectives. *Universe*, 4(11):128, nov 2018.

[18] Antonella Castellina and. AugerPrime: the pierre auger observatory upgrade. *EPJ Web of Conferences*, 210:06002, 2019.

[19] A. D. Filonenko. Radio emission from extensive air showers. *Phys. Usp.*, 58(7):633–669, 2015.

[20] Tim Huege. Radio detection of extensive air showers. *Nuclear Instruments and Methods in Physics Research Section A: Accelerators, Spectrometers, Detectors and Associated Equipment*, 876:9–12, dec 2017.

[21] Jaime Álvarez-Muñiz, Rafael Alves Batista, Aswathi Balagopal V., Julien Bolmont, Mauricio Bustamante, Washington Carvalho, Didier Charrier, Ismaël Cognard, Valentin Decoene, Peter B. Denton, Sijbrand De Jong, Krijn D. De Vries, Ralph Engel, Ke Fang, Chad Finley, Stefano Gabici, QuanBu Gou, Junhua Gu, Claire Guépin, HongBo Hu, Yan Huang, Kumiko Kotera, Sandra Le Coz, Jean-Philippe Lenain, GuoLiang Lü, Olivier Martineau-Huynh, Miguel Mostafá, Fabrice Mottez, Kohta Murase, Valentin Niess, Foteini Oikonomou, Tanguy Pierog, XiangLi Qian, Bo Qin, Duan Ran, Nicolas Renault-Tinacci, Markus Roth, Frank G. Schröder, Fabian Schüssler, Cyril Tasse, Charles Timmermans, Matías Tueros, XiangPing Wu, Philippe Zarka, Andreas Zech, B. Theodore Zhang, JianLi Zhang, Yi Zhang, Qian Zheng, and Anne Zilles. The giant radio array for neutrino detection (GRAND): Science and design. *Science China Physics, Mechanics & Astronomy*, 63(1), aug 2019.

[22] GRAND Collaboration, Rafael Alves Batista, Aurélien Benoit-Lévy, Teresa Bister, Mauricio Bustamante, Yiren Chen, LingMei Cheng, Simon Chiche, Jean-Marc Colley, Pablo Correa, Nicoleta Cucu Laurenciu, Zigao Dai, Beatriz de Errico, Sijbrand de Jong, João R. T. de Mello Neto, Krijn D. de Vries, Peter B. Denton, Valentin Deocoene, Kaikai Duan, Bohao Duan, Ralph Engel, Yizhong Fan, Arsène Ferrière, QuanBu Gou, Junhua Gu, Marion Guelfand, Jianhua Guo, Yiqing Guo, Vaidhai Gupta, Claire Guépin, Lukas Gülzow, Andreas Haungs, Haoning He, Eric Hivon, Hongbo Hu, Xiaoyuan Huang, Yan Huang, Tim Huege, Wen Jiang, Ramesh Koirala, Kumiko Kotera, Jelena Köhler, Bruno L. Lago, Sandra Le Coz, François Legrand, Antonios Leisos, Rui Li, Cheng Liu, Ruoyu Liu, Wei Liu, Pengxiong Ma, Oscar Macias, Frédéric Magnard, Olivier Martineau-Huynh, Ananstasiia Mikhno, Pragati Mitra, Miguel Mostafá, Fabrice Mottez, Jean Mouette, Kohta Murase, Valentin Niess, Stavros Nonis, Shoichi Ogio, Foteini Oikonomou, Tanguy Pierog, Lech Wiktor Piotrowski, Pierre Poisvert, Simon Prunet, Xiangli Qian, Markus Roth, Takashi Sako, Harm Schoorlemmer, Bart Steeman, Dániel Szálas-Motesiczky, Szymon Sławiński, Anne Timmermans, Charles Timmermans, Apostolos Tsirigotis, Matías Tueros, Shen Wang, Xiangyu Wang, Xu Wang, Daming Wei, Feng Wei, Xiangping Wu, Xuefeng Wu, Xin Xu, Xing Xu, Lili Yang, Xuan Yang, Qiang Yuan, Philippe Zarka, Houdun Zeng, Chao Zhang, Jianli Zhang, Kewen Zhang, Pengfei Zhang, Songbo Zhang, and Hao Zhou. The giant radio array for neutrino detection (grand) collaboration – contributions to the 38th international cosmic ray conference (icrc 2023), 2023.

[23] S J Sciutto. Aires a system for air shower simulations. user's guide and reference manual. 2019.

[24] Jonathan L. Feng, Iftah Galon, Felix Kling, and Sebastian Trojanowski. ForwArd search ExpeRiment at the LHC. *Physical Review D*, 97(3), feb 2018.

[25] R. L. Workman et al. Review of Particle Physics. *PTEP*, 2022:083C01, 2022.

[26] Colin Baus, Ralph Engel, Tanguy Pierog, Ralf Ulrich, and Michael Unger. Anomalous Longitudinal Shower Profiles and Hadronic Interactions. In *32nd International Cosmic Ray Conference*, volume 2, pages 206–209, 11 2011.

[27] Oliver Fischer, Baibhab Pattnaik, and José Zurita. Testing heavy neutral leptons in cosmic ray beam dump experiments. *Journal of High Energy Physics*, 2023(7), jul 2023.

[28] Benoit Revenu and Vincent Marin. Coherent radio emission from the cosmic ray air shower sudden death, 2013.

Appendix A

Longitudinal Photon Distributions

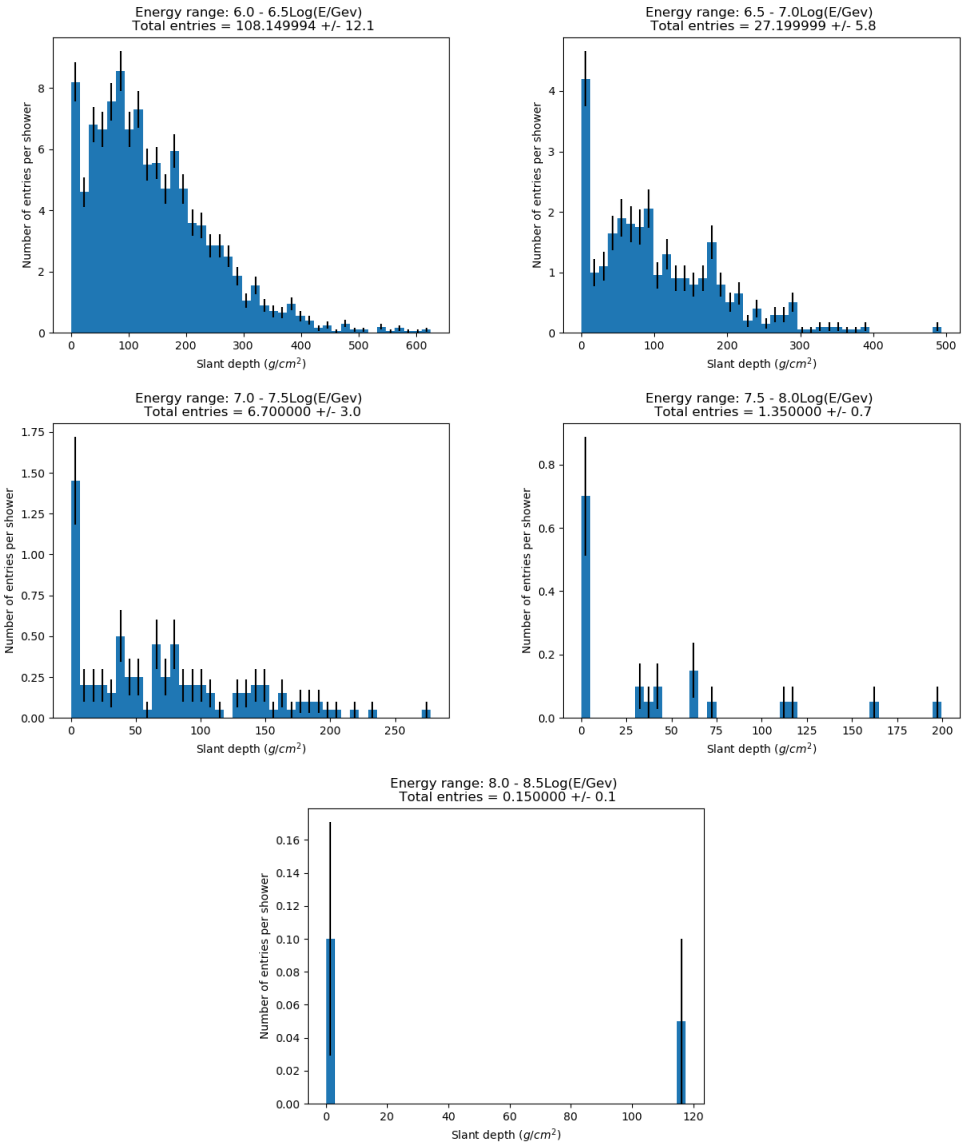

Figure A.1: Longitudinal distribution of high energy photons (split in several energy bins) in 10^{18} eV air showers with $\theta_z = 60°$. Averaged over 20 showers. A total of 143.55 ± 21.7 photons above 10^{15} eV were created. The average shower maximum in slant depth is at 748.74 ± 13.79 g/cm^2.

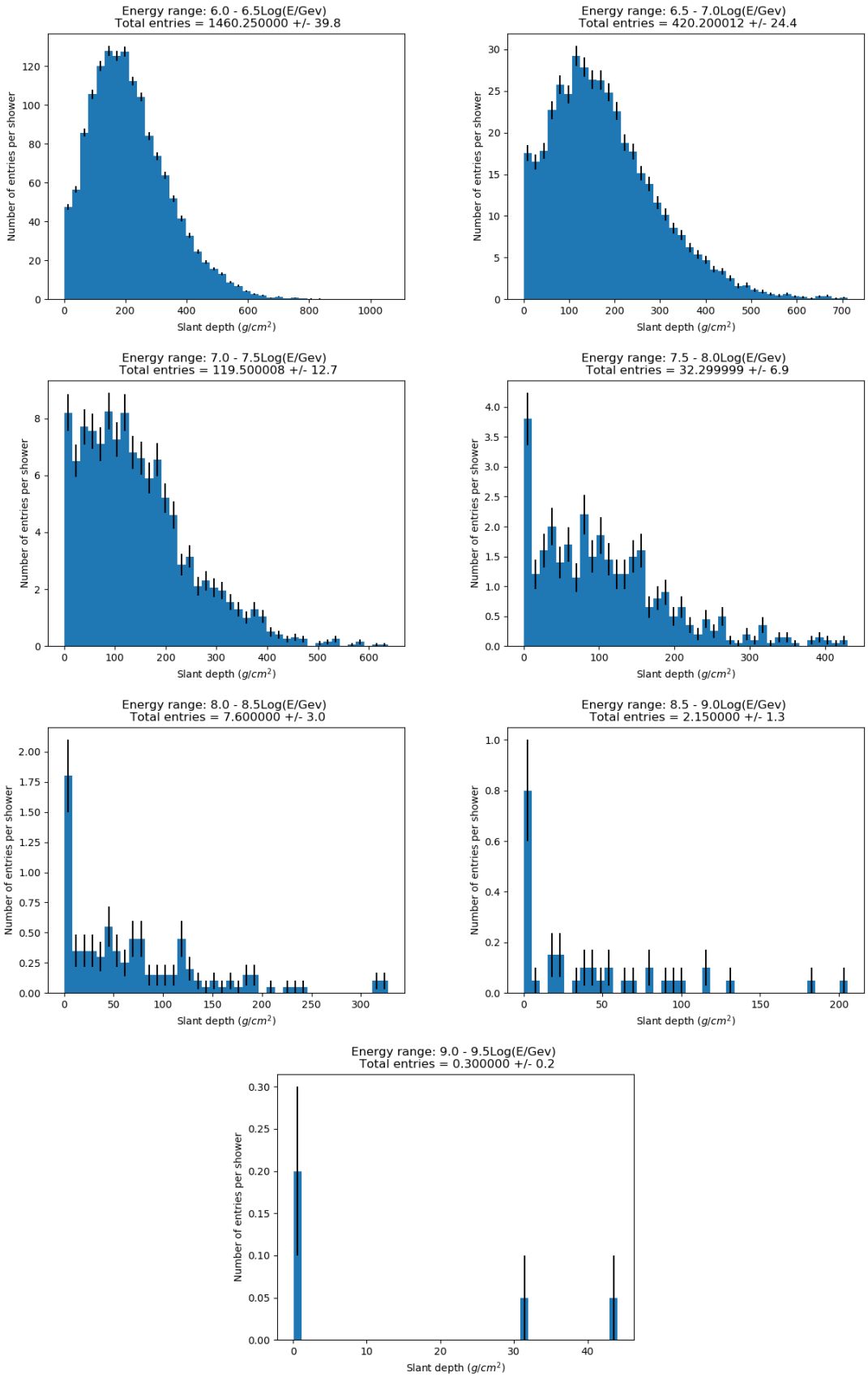

Figure A.2: Longitudinal distribution of high energy photons (split in several energy bins) in 10^{19} *eV air showers with* $\theta_z = 60°$*. Averaged over 20 showers. A total of* 2042.3 ± 88.3 *photons above* 10^{15} *eV were created. The average shower maximum in slant depth is at* 821.36 ± 8.8 g/cm^2*.*

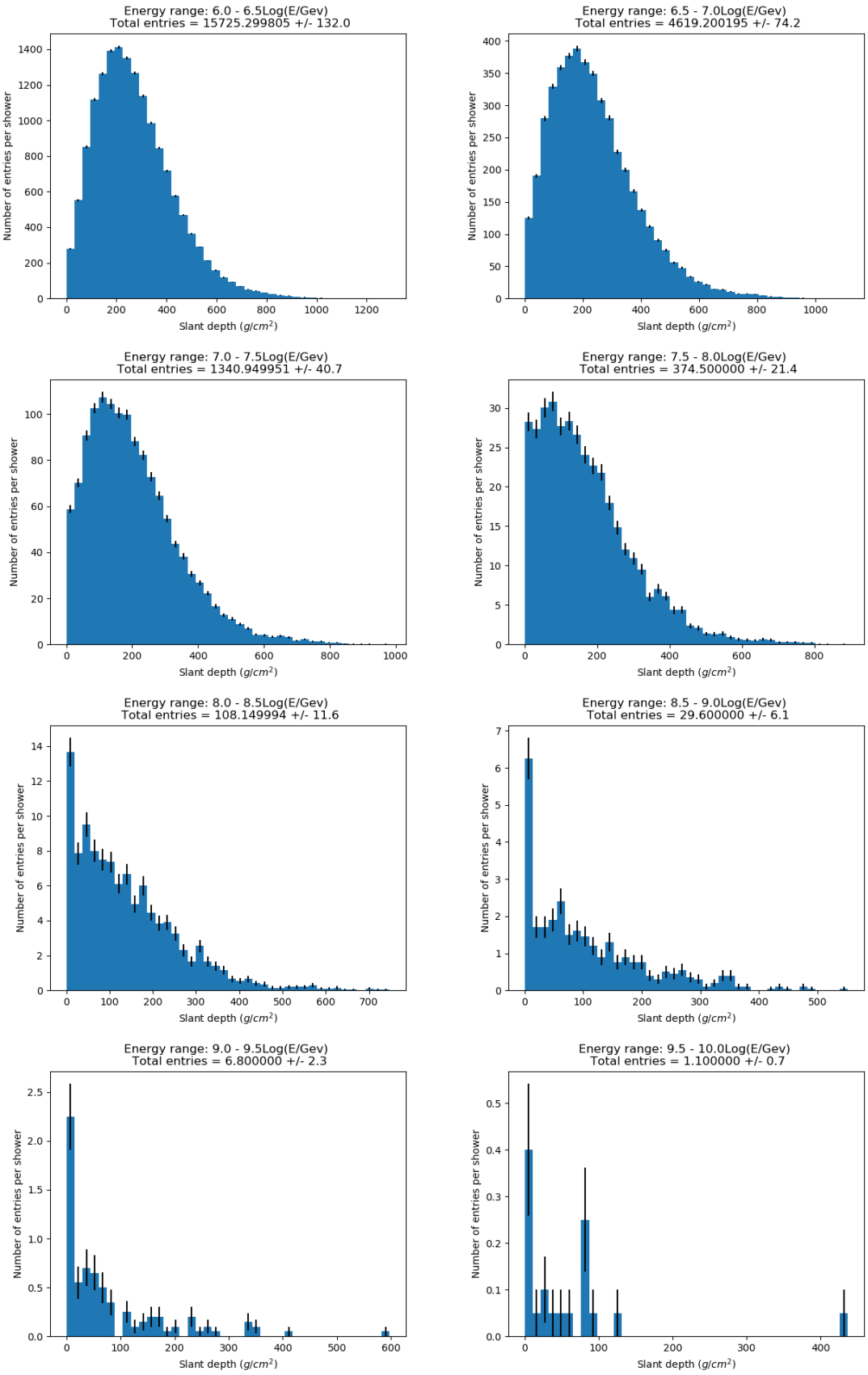

Figure A.3: Longitudinal distribution of high energy photons (split in several energy bins) in 10^{20} *eV air showers with* $\theta_z = 60°$*. Averaged over 20 showers. A total of* 22205.6 ± 289 *photons above* 10^{15} *eV were created. The average shower maximum in slant depth is at* 876.19 ± 12.8 g/cm^2*.*

Appendix B

Dark Photon Energy and Decay Histograms

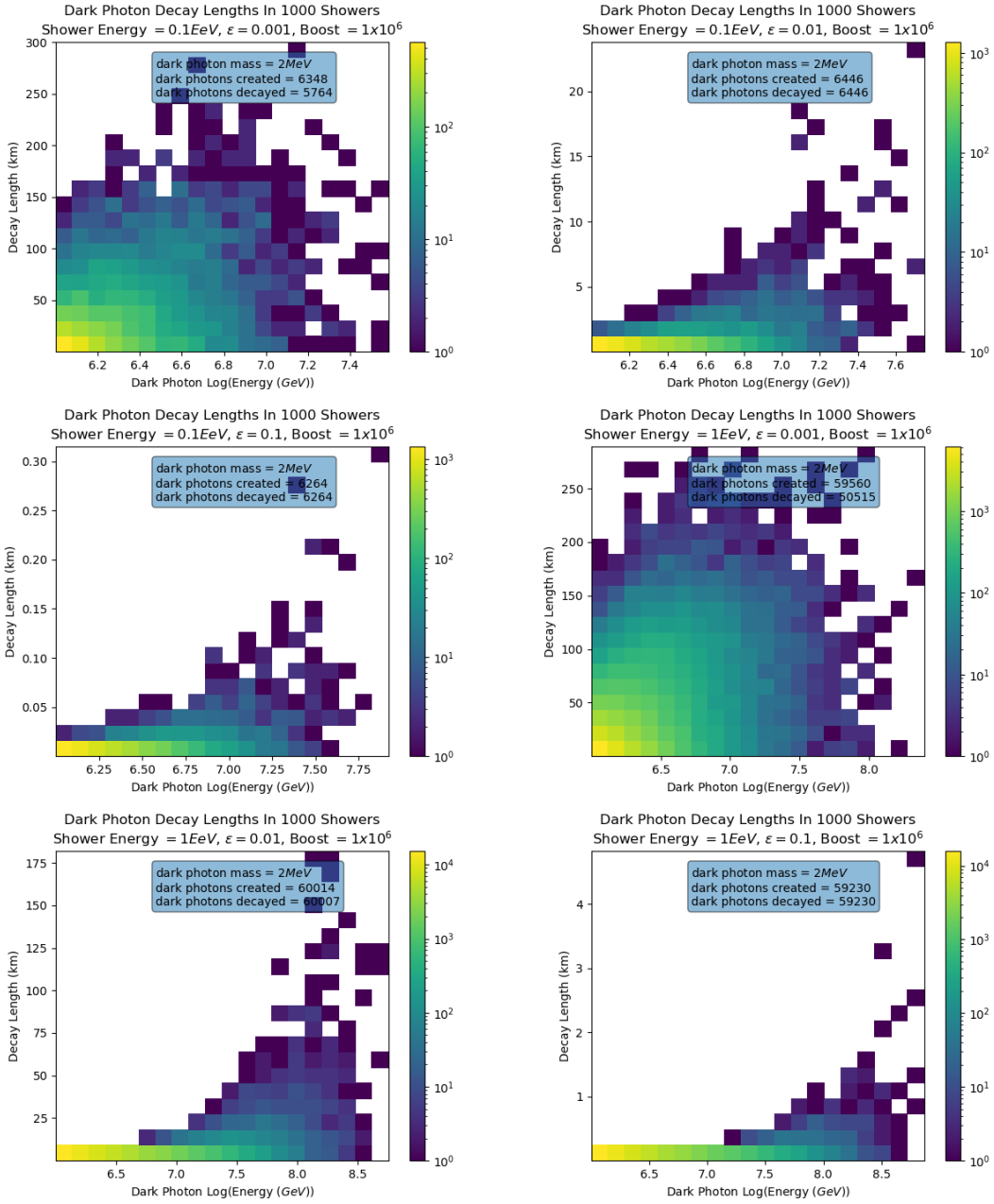

Figure B.1: Decay length/energy histograms of high energy photons produced in 1000 highly inclined air showers ($\theta_z = 80°$) for several values of $E_{primary}$ and ϵ.